UCRL-JRNL-225859

Organics Captured from Comet Wild 2 by the Stardust Spacecraft

S. A. Stanford, J. Aleon, C. M. O'D. Alexander, T. Araki, S. Bajt, G. A. Baratta, J. Borg, J. R. Brucato, M. J. Burchell, H. Busemann, A. Butterworth, S. J. Clemett, G. Cody, L. Colangeli, G. Cooper, L. D'Hendecourt, Z. Djouadi, J. P. Dworkin, G. Ferrini, H. Fleckenstein, G. Flynn, I. A. Franchi, M. Fries, M. K. Gilles, D. P. Glavin, M. Gounelle, F. Grossemy, C. Jacobsen, L. P. Keller, A. L. D. Kilcoyne, J. Leitner, G. Matrajt, A. Meibom, V. Mennella, S. Mostefaoui, L. R. Nittler, M. E. Palumbo, F. Robert, A. Rotundi, C. J. Snead, M. K. Spencer, A. Steele, T. Stephan, T. Tyliszczak, A. J. Westphal, S. Wirick, B. Wopenka, H. Yabuta, R. N. Zare, M. Zolensky

November 6, 2006

Science

Disclaimer

Organics Captured from Comet Wild 2 by the Stardust Spacecraft

Scott A. Sandford,[1 *] Jérôme Aléon,[2] Conel M. O'D. Alexander,[3] Tohru Araki,[4] Sasa Bajt,[5] Giuseppe A. Baratta,[6] Janet Borg,[7] John P. Bradley,[8] Donald E. Brownlee,[9] John R. Brucato,[10] Mark J. Burchell,[11] Henner Busemann,[3] Anna Butterworth,[12] Simon J. Clemett,[13] George Cody,[14] Luigi Colangeli,[10] George Cooper,[15] Louis D'Hendecourt,[7] Zahia Djouadi,[7] Jason P. Dworkin,[16] Gianluca Ferrini,[17] Holger Fleckenstein,[18] George J. Flynn,[19] Ian A. Franchi,[20] Marc Fries,[14] Mary K. Gilles,[21] Daniel P. Glavin,[16] Matthieu Gounelle,[22] Faustine Grossemy,[7] Chris Jacobsen,[18] Lindsay P. Keller,[23] A. L. David Kilcoyne,[21,24] Jan Leitner,[25] Graciela Matrajt,[9] Anders Meibom,[22] Vito Mennella,[10] Smail Mostefaoui,[22] Larry R. Nittler,[3] Maria E. Palumbo,[6] Dimitri A. Papanastassiou,[26] François Robert,[22] Alessandra Rotundi,[27] Christopher J. Snead,[12] Maegan K. Spencer,[28] Frank J. Stadermann,[29] Andrew Steele,[14] Thomas Stephan,[25] Peter Tsou,[26] Tolek Tyliszczak,[21,24] Andrew J. Westphal,[12] Sue Wirick,[18] Brigitte Wopenka,[30] Hikaru Yabuta,[14] Richard N. Zare[28], and Michael E. Zolensky[31]

[1] Astrophysics Branch, NASA-Ames Research Center, Moffett Field CA 94035 USA

[2] Glenn T. Seaborg Institute, Lawrence Livermore National Laboratory, Livermore, CA 94550 USA; Centre de Recherches Pétrographiques et Géochimiques, Vandoeuvre-les-Nancy FRANCE

[3] Dept. of Terrestrial Magnetism, Carnegie Institution, Washington, D.C. 20015-1305 USA

[4] Department of Physics, North Carolina State University, Raleigh, NC 27695 USA

[5] Physics and Advanced Technologies, Lawrence Livermore National Laboratory, Livermore, CA 94550 USA

[6] INAF - Osservatorio Astrofisico di Catania, Via Santa Sofia 78, 95123 Catania ITALY

[7] Institut d'Astrophysique Spatiale; Campus, 91405 Orsay Cedex FRANCE

[8] Institute of Geophysics and Planetary Physics, Lawrence Livermore National Laboratory, Livermore, CA. 94550 USA

[9] Dept. of Astronomy, Univ. of Washington, Seattle, WA 98195 USA

[10] INAF - Osservatorio Astronomico di Capodimonte, Via Moiariello 16, 80131 Napoli ITALY

[11] School of Physical Sciences, Univ. of Kent, Canterbury, Kent CT2 7NH UK

[12] Space Sciences Laboratory, University of California @ Berkeley, Berkeley, CA 94720-7450 USA

[13] ERC, Inc. / NASA Johnson Space Center, Houston, Texas 77058 USA

[14] Geophysical Laboratory, Carnegie Institution of Washington, Washington DC, 20015 USA

[15] Exobiology Branch, NASA-Ames Research Center, Moffett Field, CA 94035 USA

[16] Goddard Center for Astrobiology, NASA-Goddard Space Flight Center, Greenbelt, MD 20771 USA

[17] Novaetech s.r.l., Città della Scienza, via Cordoglio 57d, 80124 Napoli ITALY

[18] Physics and Astronomy Dept., SUNY at StonyBrook, StonyBrook, NY 11794-3800 USA

[19] Dept. of Physics, SUNY Plattsburgh, Plattsburgh, NY 12901 USA

[20] PSSRI, Open University, Milton Keynes, MK7 6AA UK

[21] Chemical Science Division, Lawrence Berkeley National Laboratory, Berkeley, CA 94720-8225 USA

[22] Laboratoire d'Etude de la Matiere Extraterrestre, Muséum National d'Histoire Naturelle, Paris FRANCE; Impacts & Astromaterials Research Center (IARC), Dept. of Mineralogy, Natural History Museum, Cromwell Road, London, UK

[23] NASA-Johnson Space Center, Houston, TX 77058 USA

[24] Advanced Light Source, Lawrence Berkeley National Laboratory, Berkeley, CA 94720-8225 USA

[25] Institut für Planetologie, Westfälische Wilhelms-Universität Münster, Wilhelm-Klemm-Str. 10, 48149 Münster GERMANY

[26] Science Division, Jet Propulsion Laboratory, 4800 Oak Grove Drive, Pasadena, CA 91109 USA

[27] Dip. Scienze Applicate, Università degli Studi di Napoli “Parthenope”, Napoli 80133 ITALY

[28] Department of Chemistry, Stanford University, Stanford, California 94305-5080 USA

[29] Dept. of Physics and McDonnell Center for the Space Sciences, Washington University, St. Louis, MO 63130 USA

[30] Dept. of Earth and Planetary Sciences and McDonnell Center for the Space Sciences, Washington University, St. Louis, MO 63130-4899 USA

[31] 1KT, NASA-Johnson Space Center, Houston, Texas 77058 USA

* - Author to whom correspondence should be addressed:
Scott Sandford
NASA/Ames Research Center
Astrophysics Branch
Mail Stop 245-6
Moffett Field, CA 94035 USA
Phone: 650-604-6849
Fax: 650-604-6779
Email: ssandford@mail.arc.nasa.gov

One Sentence Summary: Samples from Comet Wild 2 contain a complex population of organic compounds that differ in significant ways from the organic populations seen in other extraterrestrial samples.

Abstract

Organics found in Comet Wild 2 samples show a heterogeneous and unequilibrated distribution in abundance and composition. Some organics are similar, but not identical, to those in interplanetary dust particles (IDPs) and carbonaceous meteorites. A class of aromatic-poor organic material is also present. The organics are rich in O and N compared to meteoritic organics. Aromatic compounds are present, but the samples tend to be relatively poorer in aromatics than meteorites and IDPs. D and ^{15}N suggest that some organics have an interstellar/protostellar heritage. While the variable extent of modification of these materials by impact capture is not yet fully constrained, a remarkably diverse suite of organic compounds is present and identifiable within the returned samples.

Comets are small bodies that accreted in the outer Solar System during its formation *(1)* and thus may consist of preserved samples of the 'starting materials' from which the Solar System was made. Organic materials are expected to be present in cometary samples *(2)* and may include molecules made and/or modified in stellar outflows, the interstellar medium, and the protosolar nebula, as well as by parent body processing within the comet. The presence of organic compounds in comets and their ejecta is of astrobiological interest since their delivery to the early Earth may have played an important role in the origin of life on Earth *(3)*.

An overview of the Stardust Mission and the collection and recovery of Wild 2 samples is provided elsewhere *(4,5)*. We describe the results obtained from the returned samples by the Stardust Organics Preliminary Examination Team (PET). Samples were studied using a wide range of analytical techniques, including two-step laser desorption laser ionization mass spectrometry (L^2MS), Liquid Chromatography with UV Fluorescence Detection and Time of Flight Mass Spectrometry (LC-FD/TOF-MS), Scanning Transmission X-ray Microscopy (STXM), X-ray Absorption Near Edge Spectroscopy (XANES), infrared and Raman spectroscopy, Ion Chromatography with conductivity detection (IC), Secondary Ion Mass Spectrometry (SIMS), and Time-of-Flight Secondary Ion Mass Spectrometry (TOF-SIMS) *(6)*. These techniques provide a wealth of information about the chemical nature and relative abundance of the organics in the samples. Our results are compared to organic materials found in primitive meteorites and interplanetary dust particles (IDPs) collected in the stratosphere, as well as to astronomical and spacecraft observations of comets.

Despite some uncertainties associated with the presence of contaminants and alteration of the samples during the capture process, considerable information about the nature of the organics in the samples can be determined.

Some organic-containing contaminants are present in the returned sample collectors, but they are of low enough abundance or are sufficiently well characterized that they can be distinguished from the organics in the cometary materials in the returned samples *(6)*. For example, the aerogel collector medium, which consists predominantly of amorphous SiO_2, contains from a quarter to a few weight percent C. However, nuclear magnetic resonance studies indicate that this C is largely in the form of simple Si-CH_3 groups easily distinguishable from the cometary organics described below. It should be noted that not all the collected organics in the samples will be fully representative of the original cometary material since some may have been modified during impact with the aerogel collectors. There is evidence that at least some organic compounds were generated or altered by impact heating of this material *(6)*.

Multiple experimental techniques demonstrate that the samples contain polycyclic aromatic hydrocarbons (PAHs). Laser desorption - laser ionization mass spectrometry (L^2MS) spectra obtained from individual particles and in aerogel along impact tracks split lengthwise show PAHs and their alkylated derivatives. Two distinct types of PAH distributions along tracks can be distinguished from the low backgrounds of PAHs present in the aerogel (see Fig S1 and S2). In some cases benzene and naphthalene (1-2 ring PAHs, including alkylation out to several CH_3 additions) are observed in the absence of moderate mass 3-6 ring PAHs (Fig S1). These distributions are uncharacteristic of meteorites and IDPs, but resemble pyrolysis products of meteoritic macromolecular organics and are observed in high-power laser L^2MS measurements of preflight and Stardust witness aerogel tiles *(6)*, raising the question about how many of the lower mass PAHs originate from impact processing of C original to the aerogel.

The second type of the PAH population shows complex distributions that resemble those seen in meteorites and IDPs (Fig S2A). For example, Track 16 has a surface covered relatively uniformly with aromatic molecules. The organic mass distribution in this track was intermediate between typical spectra from primitive chondrites and individual IDPs. In the 78–300 amu mass range, the predominant observed species are naphthalene ($C_{10}H_8$; 2 rings; 128 amu), phenanthrene ($C_{14}H_{10}$; 3 rings; 178 amu), and pyrene ($C_{16}H_{10}$; 4 rings; 202 amu) along with their alkylated homologs extending up to at least C_4-alkyl. This distribution strongly resembles that of matrix material in the Murchison carbonaceous chondrite and some IDPs *(7)*. However, additional peaks not accounted for by simple 2-, 3-, and 4- ring C_n-alkyl-aromatics implies a more diverse suite of organics than found in Murchison. Peaks at 101, 112, 155, and 167 amu, inconsistent with simple PAHs, were observed when an attenuated laser photoionization pulse was used to minimize photofragmentation. These peaks could be due to O- and N-substituted aromatic species having hetero-functionality external to the aromatic structure, i.e., not N- or O-heterocyclics. Similar mass peaks have been observed in several IDPs *(7)*. The similarity to IDPs extends to masses beyond 300 amu; several track spectra show mass envelopes extending up to 800 amu with both odd and even mass peaks (Fig S2B). Such high mass envelopes in IDPs have been attributed to polymerization of smaller aromatics within the samples by radiation processing during their extended exposure to interplanetary space or heating during atmospheric entry. Modification of the original PAH population by heating may also explain the higher mass envelopes observed in these Stardust impact tracks.

PAHs were also seen by Time-of-Flight Secondary Ion Mass Spectrometry (TOF-SIMS) analyses of a terminal particle extracted from aerogel (Track 44, Grain 4), a dissected aerogel keystone with a particle track split down the middle (Track 21), and residues found in a large crater on Al foil C2009N. All PAHs were correlated to the presence of grains or the impact feature (see Fig S2b,c). Cometary samples from track and terminal particles typically show a steep decrease in PAH abundances with increasing number of C atoms in TOF-SIMS data, but this dependence is weaker for the crater residue (see Fig S2a). This fractionation may be due to preferential loss of smaller PAHs during impact on the foil compared to the less violent deceleration into aerogel.

Aromatic materials are also seen using Raman spectroscopy. Raman spectra, acquired for 12 Stardust particles extracted from tracks 13 (1 particle), 17 (2 particles) and 35 (9 particles), are dominated by two broad bands centered at ~1360 Δcm^{-1} and ~1580 Δcm^{-1} (Fig 1). These “D” and “G” bands, respectively, are characteristic of "disordered carbonaceous material" - graphite-like sp^2-bonded carbon in the form of condensed carbon rings. Relative peak sizes, peak positions, and widths of the D and G bands reflect the degree of disorder of the material and can provide constraints on the degree of thermal metamorphism experienced by organic materials *(8,9)*.

The Raman spectra of the 12 Stardust particles are qualitatively similar to those of many IDPs and primitive meteorites (Fig 1), indicating the presence of relatively unmetamorphosed organic matter. The G band parameters of the Stardust samples span the range observed in IDPs and meteorites (Fig 1B). It is not clear whether this variation reflects heterogeneity in the cometary samples or variable processing during aerogel impact. However, the presence of points in the upper left of the plot indicates that at least some organics were captured with relatively little alteration. A variety of carbonaceous materials exhibit the D and G bands, including disordered graphite, large PAHs, and "kerogens" (aromatic moieties linked together in a disordered fashion). These materials contain condensed aromatic rings, but differ in chemical composition. In addition to C and H, meteoritic macromolecular organics contain substantial amounts of O, N, and S, both in the aromatic rings and in cross-linked side chains. Raman spectra can reflect such compositional differences in the overall fluorescent background of the spectrum. Many Raman spectra of Stardust particles are characterized by very high and increasing backgrounds similar to the spectra obtained from Type 2 kerogen, some deuterium-rich IDPs *(10)*, and primitive meteorites, indicating that the samples may be rich in non-carbon heteroatoms such as N, as confirmed by XANES and SIMS results (see below, and ref *(11)*). In a few cases, aromatic materials have also been identified by infrared spectroscopy *(6)*.

Infrared (IR) spectra taken from tracks and individual extracted particles provide evidence for the presence of other, non-aromatic chemical functional groups. IR spectra of particles and tracks often contain absorption features at 3322 cm^{-1} (–OH), 3065 cm^{-1} (aromatic CH), 2968 cm^{-1} ($-CH_3$), 2923 cm^{-1} ($-CH_2-$), 2855 cm^{-1} ($-CH_3$ and $-CH_2-$), and 1706 cm^{-1} (C=O) (Fig 2 and Fig S5-S6*, 12*). When present, these features are particularly intense along the track walls. IR reflectance spectra of individual grains removed from impact tracks and pressed into Au substrates exhibit similar absorption features. One particle (Track 35, Grain 26) also showed a weak 2232 cm^{-1} band possibly due to –C≡N stretching vibrations. Raman spectra of three Stardust samples (Track 35, Grain 30; Track 35, Grain 32; and (Track 41, Grain 7) are also consistent with the presence of alkane-type saturated hydrocarbons (see Fig S4). Combined, these spectra data indicate the presence of aromatic, aliphatic, carboxylic, and N-containing functional groups.

The observed -CH_2- (2923 cm^{-1})/-CH_3(2968 cm^{-1}) band depth ratios in the returned samples is typically ~2.5 *(12)*. This band depth ratio is similar to the average value from IR spectra of anhydrous IDPs *(14)*, but considerably larger than seen in macromolecular material in primitive carbonaceous chondrites (~1.1) and the diffuse interstellar medium (ISM; 1.1-1.25). This suggests that the aliphatic moieties in Wild-2 particles are longer or less branched than those in the diffuse ISM. The band depth ratio of ~2.5 corresponds to a functional group ratio of -CH_2-/-CH_3 ~ 3.7 in the Wild 2 samples, assuming typical intrinsic band strengths for these features *(13)*. The ratio of aromatic to aliphatic C-H is quite variable, with C-H stretching aromatic/aliphatic optical depth ratios ranging from below the detection limit to ~0.1 *(6)*.

C,N,O-XANES analyses of thinsections of individual grains confirm the presence of 1s-π^* transitions consistent with variable abundances of aromatic, keto/aldehydic, and carboxyl moieties, as well as amides and nitriles (Fig 3A). XANES data suggest that considerably less H- and C-substituted sp^2-bonded C (olefinic and aromatic) is present than in highly primitive chondritic organic matter. Aliphatic C likely contributes to spectral intensity around 288 eV in most of the particles. One particle (particle 1 in Fig 3A) has remarkably simple C chemistry consistent with a predominance of alcohol and/or ether moieties. However, the XANES data generally indicate complex molecular structures variably rich in heteroatoms O and N and, compared to the macromolecular material in primitive meteorites, containing additional materials that are relatively poor in aromatic and olefinic C. The high abundances of heteroatoms and the low concentration of aromatic C in these organics differ greatly from the acid insoluble organic matter in meteorites and, in terms of thermal processing, appear to be more primitive.

XANES provides quantitative estimates of atomic O/C and N/C ratios present in the various functional groups identified *(6)*. Care must be taken to account for O from any associated silicates or aerogel. Fig 3B shows that five of six organic-rich particles are richer in the heteroatoms O and N relative to both chondritic organic matter and the average composition of Comet Halley particles measured by Giotto *(16)*. The values are, however, qualitatively similar to the average O/C and N/C reported for stratospheric IDPs *(17)*. Particles with such high O/C and N/C ratios are likely to be relatively labile (see below and *(6)*).

Particles 2 and 3 are particularly rich in N and exhibit abundant amide C in their XANES spectra (Fig 3A). The presence of N-containing compounds is further suggested by studies of collector aerogel using Liquid Chromatography with UV Fluorescence Detection and Time-of-Flight Mass Spectrometry (LC-FD/TOF-MS). While PET attention has largely focused on impacts in the aerogel and Al foils, Stardust may have returned a 'diffuse' sample of gas-phase molecules that struck the aerogel directly or that diffused away from grains after impact. To test this possibility, samples of flight aerogel were carried through a hot water extraction and acid hydrolysis procedure *(18)* to determine if primary amine compounds were present in excess of those seen in controls.

With the exception of methylamine (MA) and ethylamine (EA), all amines detected in Stardust aerogel samples Cell 2054, Aerogel Fragment 4 (hereafter C2054,4) and Cell 2086, Aerogel Fragment 1 (hereafter C2088,1) were also present in the witness coupon aerogel sample (WCARMI1CPN,9). The absolute abundances of MA and EA are much higher, and the molar ratio of MA to EA in Stardust comet-exposed aerogel (C2054,4: 1.0 ± 0.1; C2086,1: 1.8 ± 0.2) is distinct from preflight aerogel (Flight Spare Aerogel Cell E243-13C, unflown: 10 ± 3) *(6)*. The absence of MA and EA in the aerogel witness coupon suggests that these amines are cometary in origin. The concentrations of MA and EA in C2054,4 (0.6 to 2.2 parts-per-million) were similar to those present in C086,1 that was not located adjacent to a particle track, suggesting that these amines, if cometary, originate from sub-micron particles or gas that directly impacted the collector. Glycine is also present in samples C2054,4 and C086,1 at relative abundances that exceed those found in controls. This may indicate that a cometary component for this amino acid is also present. Compound specific isotope measurements will be necessary to constrain the origin of these amines. No MA, EA, or glycine was detected in non acid-hydrolyzed aerogel extracts. This suggests that these amines are present in an acid soluble bound form, rather than as a free primary amine. These results are consistent with the XANES detection of an amine rich organic polymer in some of the recovered particles.

Raman (Fig 1B), XANES (Fig 3), and isotopic *(11)* data all demonstrate that the distribution of organics (overall abundance, functionality, and relative elemental abundances of C,N,O) is heterogeneous both within particles and between particles. The STXM XANES results show variations in the physical distribution of these materials within particles, and the IR mapping of particle tracks (Fig 2) shows the presence of organic features in some impact tracks, but not others. The degree to which these variations represent heterogeneity in the original samples vs. differences in impact processing is currently not fully constrained. On the whole, the chemical variations suggest that cometary organics do not represent an equilibrated reservoir of materials.

Most of the organic material in meteorites is in insoluble macromolecular phases. In contrast, the Stardust samples show evidence of abundant, relatively labile organics. In many cases the organic components that produce the –OH, $-CH_3$, $–CH_2-$, and C=O IR absorption bands extends well beyond the visible edge of the track (Fig 2). This suggests that the incoming particles contained organics that volatilized during impact and diffused into the surrounding aerogel. This material is unlikely to be due to impact-altered C from the aerogel because similar tracks are seen in the same aerogels that show no IR-detectable organics beyond those seen in the original aerogel (Fig 2). All impacting particles had identical velocities, and tracks of similar length probably had similar impact energies. Consequently, similar amounts of organics would be expected in all tracks if this material came solely from reprocessing of C in the aerogel. Also, if impact-driven oxidation of C in the aerogel was occurring, the C=O band might be expected to be seen in and around all tracks, but this feature is only seen in tracks with the other organic features. Finally, locations near tracks show no deficits of the $–CH_3$ original to the aerogel, implying the original C has not been significantly converted to other forms.

Hydrogen isotopic measurements were made by SIMS in fragments of 5 particles *(11)*. D/H enrichments up to three times terrestrial were observed in 3 of 5 measured samples. D enrichments are often seen in meteoritic and IDP organics and are thought to be due to materials with an interstellar/protostellar chemical heritage *(19,20,21)*. In all cases, the D-rich H is heterogeneously distributed within the samples and is associated with C, indicating it is organic. The elevated D/H ratios are comparable to those of many IDPs and meteoritic samples, although none of the cometary samples examined to date have shown ratios as extreme as the most anomalous values measured in some IDPs, meteorites, and some cometary coma gases.

Isotopic anomalies are also observed in C and N *(11)*. As with IDPs and meteorites, these anomalies often appear in the form of 'hot spots' that differ from the surrounding particle. Nano-SIMS ion imaging demonstrates that N and S are associated with organic molecules (Fig 4). The samples show a distribution of N/C ratios ranging from 0.005 to values approaching 1. Some particles exhibit the entire range of values, while others fall more uniformly at the high N/C end of the range, consistent with the XANES data (Fig 3B). However, there are regions with high C content that are not rich in N. Sulfur is typically associated with C and N, but is also distributed in small hotspots presumably due to sulfides, which are commonly seen in the returned samples *(22)*.

When observed, the D and/or ^{15}N enhancements provide clear evidence of a cometary origin for the organics and suggest that cometary organics contain a population with an interstellar/protostellar chemical heritage. Particles with measured isotopic anomalies are represented among the samples studied by other techniques by the Organics PET – for example, FC9,0,13,1,0 (Track 13, Grain 1) (Particle 6 in Fig 3) was examined by XANES, and particles Track 13, Particle 1; Track 17, Grain 1; Track 35, Grain 25 were measured by Raman.

In terms of sample heterogeneity, the organics found in Stardust samples are similar to stratospheric IDPs and primitive meteorites. Like meteoritic organic matter, they contain both aromatic and non-aromatic fractions. However, the Stardust samples exhibit a greater range of compositions (higher O and N concentrations), include an abundant organic component that is poor in aromatics, and a more labile fraction (possibly the same material). The non-aromatic fraction appears to be far more abundant, relative to aromatics, than is seen in meteorites. In general terms, the organics in Stardust samples are even more "primitive" than those in meteorites and IDPs, at least in terms of being highly heterogeneous and unequilibrated.

The Cometary and Interstellar Dust Analyzer (CIDA) time-of-flight mass spectrometer instrument on the Stardust spacecraft detected very few particle impacts during the flyby *(23)*. However, some of the returned mass spectra suggest the presence of particles with a nitrogen-rich chemistry and lower abundances of O, implying that nitriles or polycyanides may have been present *(23)*. While direct comparisons are not possible, studies of the samples confirm that N-rich components are present in the dust.

The presence of high O and N contents and the high ratios of $–CH_2$-/-CH_3 seen in the infrared data indicate that the Stardust organics are not similar to the organic materials seen in the diffuse ISM, which look more similar to the insoluble macromolecular material seen in primitive meteorites, but with even lower O/C ratios *(24)*. This suggests that the Stardust organics are not the direct result of stellar ejecta or diffuse ISM processes, but rather result from dense cloud and/or protosolar nebular processes. The high O and N contents, lower aromatic contents, and elevated $–CH_2$-/-CH_3 ratios are all qualitatively consistent with what is expected from radiation processing of astrophysical ices and the polymerization of simple species like HCO, H_2CO, HCN, etc. *(15,25,26)*.

The Stardust samples clearly contain an organic component that is more labile than the materials seen in meteorites and IDPs. These labile materials may be absent from stratospheric IDPs because they are lost during atmospheric entry heating and/or are destroyed or modified by radiation during the IDPs' transit from parent body to Earth. Given the O- and N-rich nature of the Stardust materials, these labile organics could represent a class of materials that have been suggested as parent molecules to explain the extended coma sources of some molecular fragments like CN *(27,28)*. The high O/C and N/C ratios of the samples fall well outside the range of most meteorites and, interestingly enough, reach higher values than those observed at comet Halley by the Giotto spacecraft *(16)*. In this respect, some of the returned material appears to represent a new class of organics not previously observed in other extraterrestrial samples.

REFERENCES AND NOTES

1. M. C. Festou, H. U. Keller, H. A. Weaver, Eds., Comets II, (Univ. Arizona Press, Tucson, 2004).

2. A. H. Delsemme, Advances in Space Research 12, 5 (1992).

3. C. F. Chyba, C. Sagan, C., Nature 355, 125 (1992).

4. D. E. Brownlee et al., J. Geophys. Res. 108, #E10, 8111, p. 1-1 (2003).

5. D. E. Brownlee et al., this issue.

6. see Supporting Online Materials.

7. S. Clemett, C. Maechling, R. Zare, P. Swan, R. Walker, Science 262, 721 (1993).

8. B. Wopenka, J. D. Pasteris, American Mineralogist 78, 533 (1993).

9. L. Bonal, E. Quirico, M. Bourot-Denise, G. Montagnac, Geochimica et Cosmochimica Acta 70, 1849 (2006).

10. B. Wopenka, EPSL 88, 221 (1988).

11. K. D. McKeegan et al., this issue.

12. L. P. Keller et al., this issue.

13. S. A. Sandford et al., Astrophys. J. 371, 607 (1991).

14. G. Matrajt et al., Astron. & Astroph. 433, 979 (2005).

15. M. P. Bernstein, S. A. Sandford, L. J. Allamandola, S. Chang, M. A. Scharberg, Astrophys. J. 454, 327 (1995).

16. J. Kissel, F. R. Krueger, Nature 326, 755 (1987).

17. G. J. Flynn, L. P. Keller, S. Wirick, C. Jacobsen, Proceedings of the 8th International Conference on X-ray Microscopy, IPAP Conf. Series 7, 315 (2006).

18. D. P. Glavin et al., Meteoritics Planetary Science 41, 889 (2006).

19. S. Messenger, Nature 404, 968 (2000).

20. J. Aléon, F. Robert, Icarus 167, 424 (2004).

21. H. Busemann et al., Science 312, 727 (2006).

22. M. E. Zolensky et al., this issue.

23. J. Kissel, F. R. Krueger, J. Silén, B. C. Clark, Science 304, 1774 (2004).

24. Y. J. Pendleton, L. J. Allamandola, Astrophys. J. Suppl. Ser. 138, 75 (2002).

25. W. A. Schutte, L. J. Allamandola, S. A. Sandford, Icarus 104, 118 (1993).

26. G. Strazzulla, G. A. Baratta, M. E. Palumbo, Spectrochim. Acta 57, 825 (2001).

27. M. J. Mumma, P. R. Weissman, S. A. Stern, in Protostars and Planets III, E. H. Levy, J. I. Lunine, M. S. Matthews, Eds. (Univ. Arizona Press, Tucson, 1993), pp. 1171-1252.

28. G. Strazzulla, Space Science Reviews 90, 269 (1999).

29. E. Quirico, J. Borg, P.-I. Raynal, G. Montagnac, L. D'Hendecourt, Planetary and Space Science 53, 1443 (2005).

30. G. A. Baratta et al., Journal of Raman Spectroscopy 35, 487 (2004).

FIGURE CAPTIONS

FIGURE 1 – A) Raman spectra of Stardust particles from Track 35, Grain 30 and Track 13, Grain 1 (top pair) compared to the spectra of organics from extraterrestrial (middle three) and terrestrial (bottom pair) carbonaceous materials with different fluorescence backgrounds. All exhibit D and G bands characteristic of disordered sp2-bonded carbon. The phyllosilicate bands below 1000 cm^{-1} in the IDP spectrum have not been seen in Stardust samples. B) The G band position and width (FWHM) of a material reflect its degree of thermal metamorphism and "structural ordering." The boundaries show the range of values from over 40 chondritic meteorites (unshaded area with dashed outline) and 40 IDPs (shaded area with solid outline) analyzed in PET Raman laboratories *(9,10,29)*. Analyzed Stardust particles (points) span the entire range seen in IDPs and meteorites. Organics in highly thermally metamorphosed meteorites plot to the lower right. The presence of Stardust points in the upper left indicates that at least some of the cometary organics are very primitive and were captured with relatively little alteration. One Stardust sample shows an unusually low G band position (below 1570 cm^{-1}), suggesting diamond-like carbon that has been amorphized, e.g., due to particle irradiation *(30)*. One-sigma error bars represent measurement reproducibility and do not include estimates of possible inter-laboratory biases.

FIGURE 2 – IR transmittance spectra obtained along a line perpendicular to cometary impact tracks (a) Track 59 and (b) Track 61. In addition to aerogel features, the spectra of Track 59 (a) display peaks at 3322 (broad), 2968, 2923, 2855, and 1706 cm^{-1} (not shown) both inside the track and extending outward into the aerogel. (b) Track 61 exhibits only the aliphatic CH stretching feature dominated by the 2968 cm^{-1} peak and (Si-O) bands (not shown) characteristic of the flight aerogel. The optical images of the same tracks, with corresponding maps to the same scale showing the intensity distribution of the 2923 cm^{-1} peak ($-CH_2-$), are displayed in (c) and (d). The false color image scale shown at the bottom is used in both maps and the black scale bars correspond to 100 μm. In both cases the entrance of the cometary particle is on the left hand side. The false color map in (c) shows an increase in intensity of the 2923 cm^{-1} $–CH_2-$ peak in and near the track. The distributions of other organics peaks are similar. In contrast, the second

track shown in (d) shows almost uniform distribution of the peak area centered at 2923 cm^{-1}, i.e., the track shows only the features of aerogel.

FIGURE 3 - A) C-XANES spectra of six thin section samples (1-6) compared to spectra of primitive (EET92042, CR2) and moderately processed (Tieschitz, L3.6) chondritic organic matter. Samples are **1**, Track 16, Grain 1, Mount 10; **2**, Track 35, Grain 16, Mount 4 ; **3**, Track 22, Grain 1, Mount 5; **4**, Track 35, Grain 32, Mount 10; **5**, Track 35, Grain 32, Mount 8 ; and **6**, (Track 13, Grain, Mount 5) (samples **4** and **5** are different thin sections of the same grain). Specific organic functional groups are highlighted (dashed lines a-f); a) (C=C at ~285.2 eV), b) (C=C-O at ~286.5 eV), c) (C=O at ~287.5 eV), d) (N-C=O at 288.2 eV), e) (O-C=O at 288.6 eV), and f) (C-O at 289.5 eV). Sample chemistry ranges enormously, with sp^2 bonded carbon varying from non-existent in **1** to modest in samples **5** and **6** (relative to chondritic organic matter). **B)** Atomic O/C and N/C for samples 1-6 derived from C,N,O-XANES analysis (black triangles) are compared to chondritic organic matter (grey squares, where the higher values corresponds to petrologic type 1 and 2 and the lower values are type 3). Average values for Comet Halley particles and stratospheric IDPs *(17)* are marked by a black star and a large solid circle, respectively. **C)** An example of a sample thin section from Track 35, Grain 32, Mount 8 (spectrum **5**) revealed as a high resolution (40 nm pixel size) STXM optical density image (scale bar = 1 μm) on the carbon 1s absorption edge.

FIGURE 4 - Distribution of C and N. A) Histograms of C/N ratios in organics in three different Stardust samples. One sample (top) shows a large spread in C/N, whereas two samples (bottom) have organics characterized by low C/N ratios, consistent with the presence of volatile organic molecules such as HCN, or their polymer counterparts. B) NanoSIMS images of the distribution of C, N, and S in a region of an aerogel sample from along Track 35 containing cometary materials. The intensity of the signal increases from blue, to red, to bright yellow. C, N, and S distributions are clearly correlated, although significant variations in their relative abundances are observed. S is also present in a population of ‘hotspots’ that likely indicate the presence of sulfides. The color scale in the S map is logarithmic, in order to show the large difference in S count rates between the organics and the sulfides. The distribution of C and N is qualitatively similar in particles both with and without ^{15}N excesses. The location labeled IOM (CCs) in the

upper left panel denotes the C/N ratio of the insoluble organic matter found in carbonaceous chondrites.

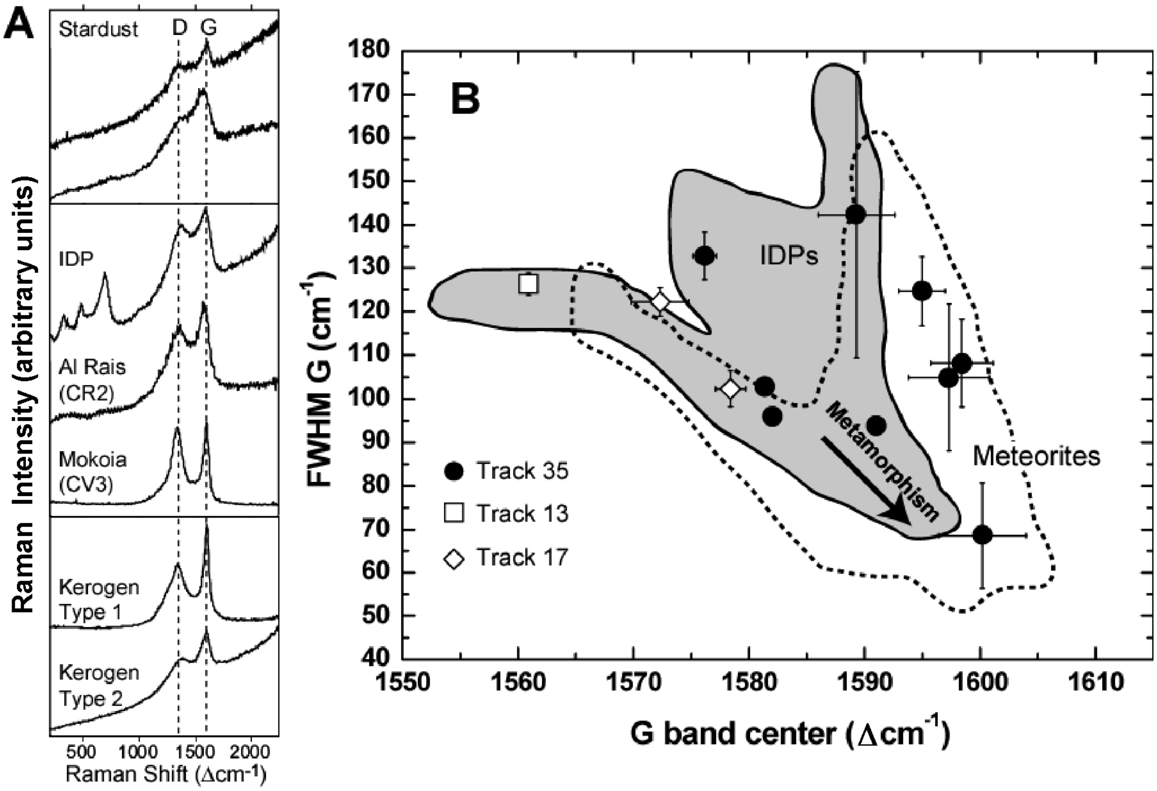
A
Stardust
D
G
IDP
Al Rais (CR2)
Mokoia (CV3)
Kerogen Type 1
Kerogen Type 2
Raman Intensity (arbitrary units)
500
1000
1500
2000
Raman Shift (Δcm-1)
B
IDPs
Meteorites
Metamorphism
● Track 35
□ Track 13
◇ Track 17
FWHM G (cm-1)
180
170
160
150
140
130
120
110
100
90
80
70
60
50
40
1550
1560
1570
1580
1590
1600
1610
G band center (Δcm-1)

FIGURE 1

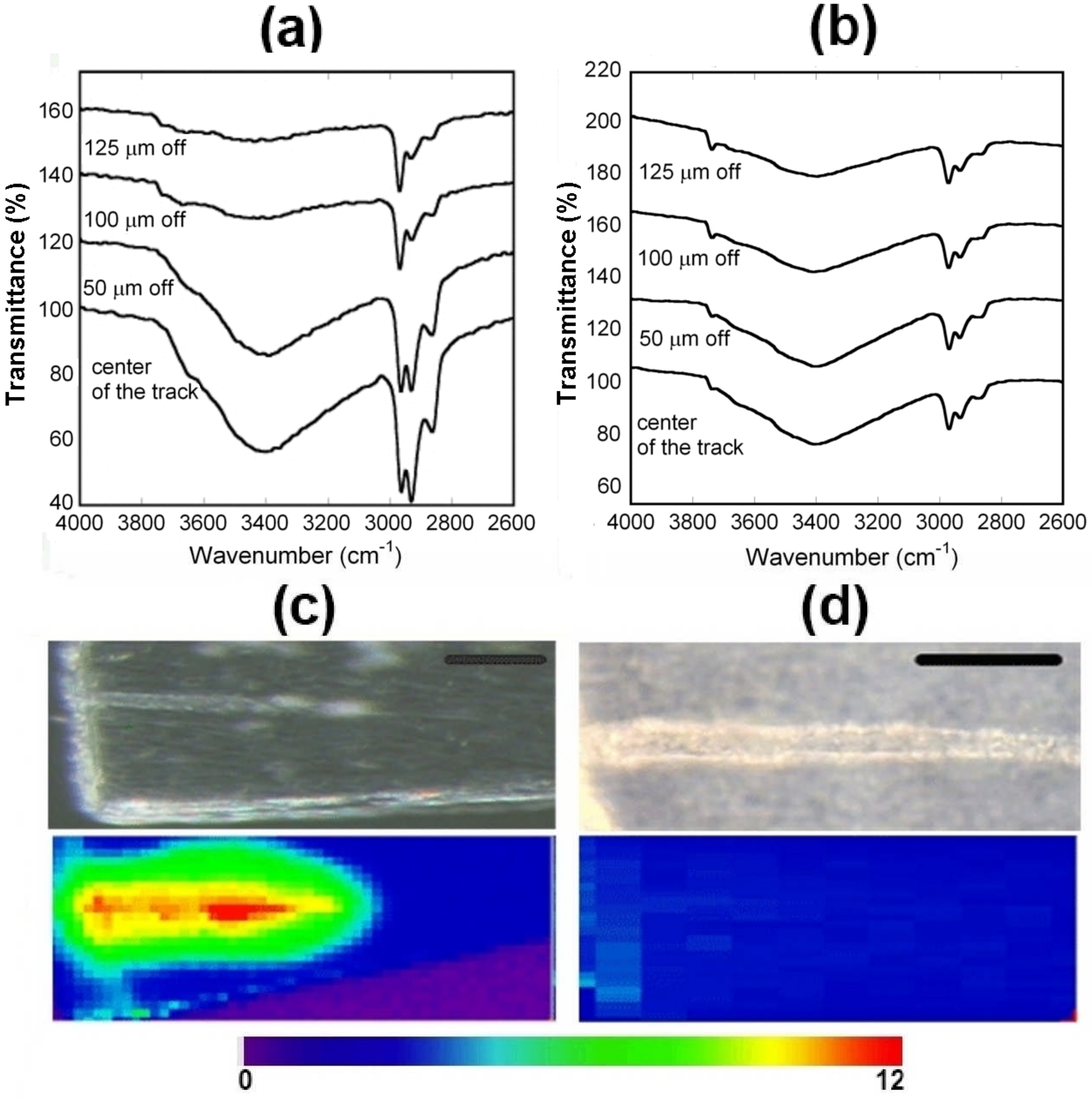
(a)
(b)
Transmittance (%)
160
140
120
100
80
60
40
125 μm off
100 μm off
50 μm off
center of the track
4000 3800 3600 3400 3200 3000 2800 2600
Wavenumber (cm^{-1})
220
200
180
160
140
120
100
80
60
(c)
(d)
0
12

FIGURE 2

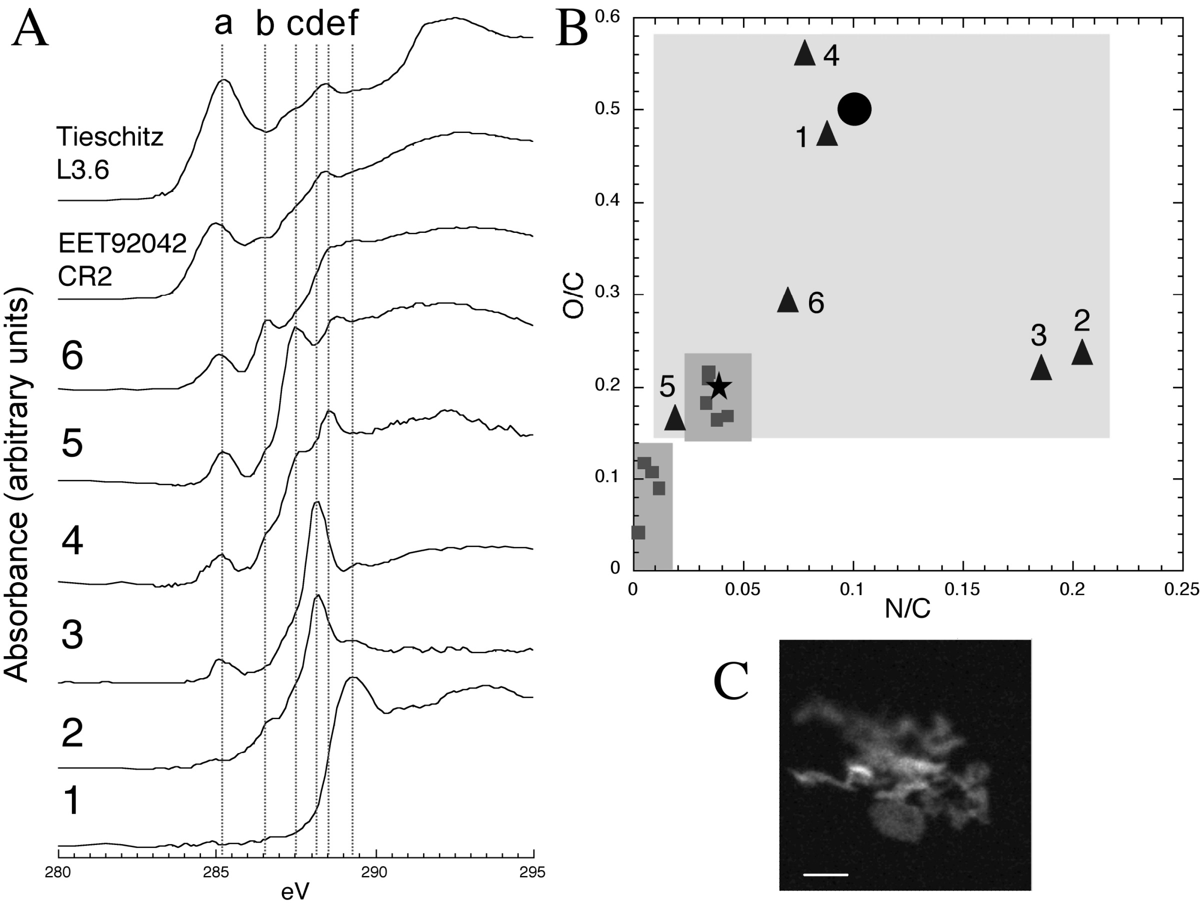
A
a b cdef
Tieschitz
L3.6
EET92042
CR2
6
5
4
3
2
1
Absorbance (arbitrary units)
280
285
290
295
eV
B
0.6
0.5
0.4
0.3
0.2
0.1
0
O/C
4
1
6
3
2
5
0
0.05
0.1
0.15
0.2
0.25
N/C
C

FIGURE 3

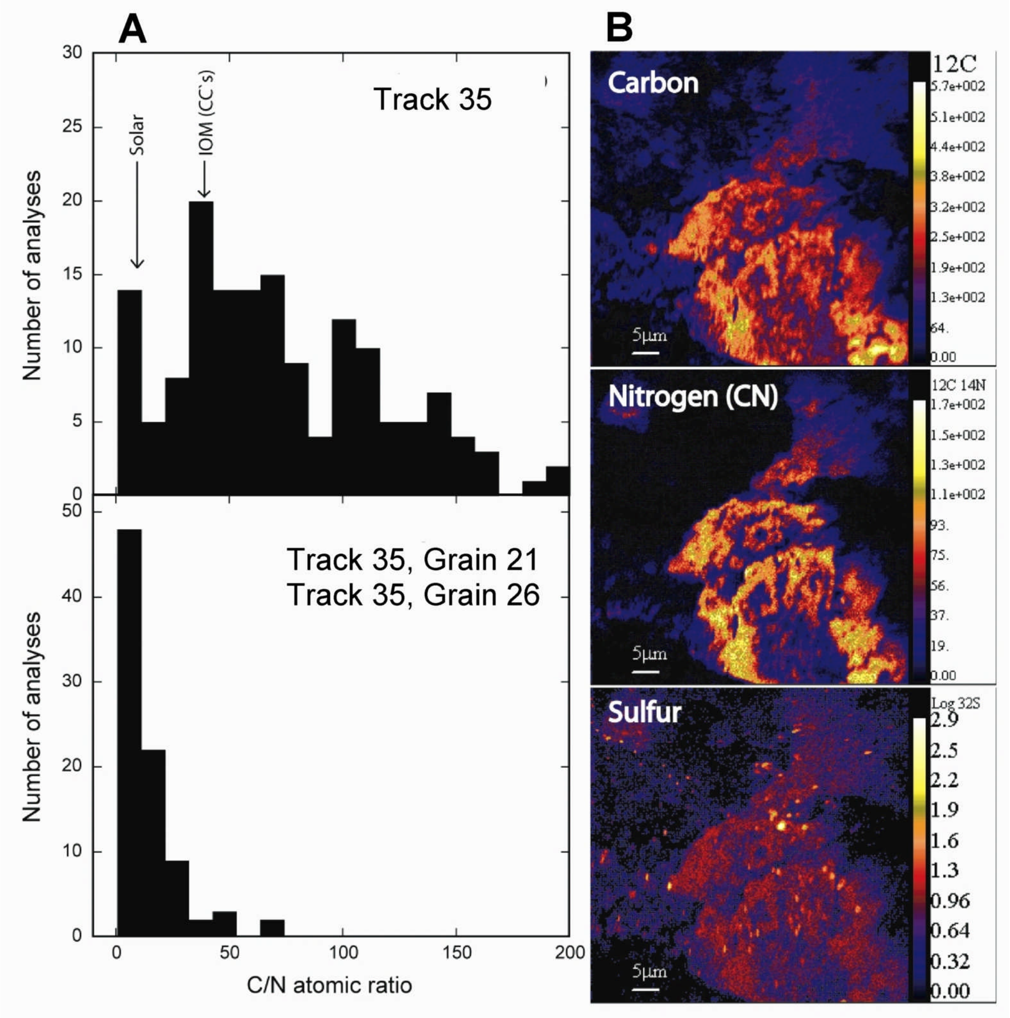
A
B
Track 35
Track 35, Grain 21
Track 35, Grain 26
Solar
IOM (CC`s)
Number of analyses
C/N atomic ratio
0
50
100
150
200
0
5
10
15
20
25
30
10
20
30
40
50
Carbon
12C
5.7e+002
5.1e+002
4.4e+002
3.8e+002
3.2e+002
2.5e+002
1.9e+002
1.3e+002
64.
0.00
Nitrogen (CN)
12C 14N
1.7e+002
1.5e+002
1.3e+002
1.1e+002
93.
75.
56.
37.
19.
0.00
Sulfur
Log 32S
2.9
2.5
2.2
1.9
1.6
1.3
0.96
0.64
0.32
0.00
5μm

FIGURE 4

MATERIALS, METHODS AND SUPPORTING DATA

Introduction

For additional references that discuss the types of organic materials expected to be present in comets, see *(S1,S2)*. For additional references discussing the role comets may have played in the origin of life, see *(S3,S4,S5)*.

Particle Extraction Techniques

Whole tracks in the aerogel collectors were extracted using techniques developed in the Westphal lab at the Space Sciences Laboratory, U. C. Berkeley *(S6)*. Glass rods (1mm diameter) are pulled to make two microneedles. The needles are held by micromanipulators that are attached to the stage of the extraction microscope. The needles cut the aerogel by repetitive "poking." The micromanipulators are driven automatically by computer. First, an angled cut is made which undercuts the deepest feature of a particular impact; then a vertical cut is made around the impact. The resulting wedge-shaped block of aerogel (a "keystone") contains the entire impact track and the terminal particles. The keystone is then removed from the collector using silicon microforks that are inserted into pre-machined holes in the keystone. For certain analytical techniques, it is desirable to slice a track into multiple cross-sections; other techniques require a sample of the bulb that has been cleaved lengthwise. These specialized samples are prepared by laying a keystone on its side and using the same aerogel cutting tools to dissect or slice wafers of the track bulb. Terminal particles were removed from some keystones by using a bent glass needle to dig a tunnel to the particle and lifting it out using the same needle. The particle then can be mounted on a number of different types of substrates suitable for a variety of analytical techniques.

Since we had no a priori means of establishing which impact tracks might contain organic materials, most samples were simply allocated more-or-less randomly to Preliminary Examination Team (PET) members as they became available. In cases where early application of an individual analytical technique demonstrated a sample contained organics, it was then possible to (i) subsequently allocate associated samples (for example, other particles from the same track) to other PET members, and/or (ii) pass the sample to another team member once the initial analysis was completed. By this process that we were able to examine a number of samples using multiple techniques.

Analytical techniques

Analytical techniques used to study the cometary samples and related control samples included:

Two varieties of two-step laser desorption laser ionization mass spectrometry *(S7,S8,S9)*, called micro--L^{2}MS and ultra-L^{2}MS,

LC-FD/TOF-MS (Liquid Chromatography with UV Fluorescence Detection and Time of Flight Mass Spectrometry; *(S10)*),

STXM (Scanning Transmission X-ray Microscopy and C, N, and O XANES (X-ray Absorption Near Edge Structure) *(S11,S12,S13)*,

Infrared and Raman Spectroscopy *(S14,S15,S16,S17,S18)*,

IC (Ion chromatography with conductivity detection; *(S19)*),

TOF-SIMS (Time-of-Flight Secondary Ion Mass Spectrometry; *(S20)*), and

SIMS (Secondary Ion Mass Spectrometry; *(S21,S22)*).

Contamination Control and Assessment

The Sample Return Capsule (SRC) touched down on January 15, 2006 in the Utah Test and Training Range on soft mud in wet conditions under a prevailing crosswind. It bounced four times on different parts of the capsule before rolling a short distance and coming to rest on the side of its backshell. Visible inspection of the SRC shortly after impact indicated it had not suffered any identifiable loss of integrity. Nevertheless, since the SRC was not hermetically sealed, atmospheric gases in the environment surrounding the descending capsule would have been drawn into the capsule interior as it underwent pressure equalization. This provides a potential entry route for contamination by heatshield ablation products as well as water and soil from the landing site. To limit such contamination a high efficiency particulate air (HEPA) filter was fitted in-line between the backshell entry vents and the canister interior.

Atmospheric samples were collected from near the heatshield and backshell air entry vents shortly after the Recovery Team arrived, and several times thereafter as the SRC was transported to the clean room in which it was disassembled. GCMS analyses of the collected gases showed no significant contributions from organic compounds with the exception of 2-propanol and 1,1,1,2-tetrafluoroethane found in gases collected after the SRC was moved into a temporary cleanroom at the UTTR. These are thought to be associated with materials used earlier to prepare the clean room. Thus, there are currently no indications that significant amounts of volatile organic contaminants were sucked into the SRC through the back vents during descent. The Wild 2 samples were further protected from gas contaminants by a filter placed on the sample canister inside the SRC. During disassembly of the SRC, this filter was observed to look pristine, indicating that the SRC did not ingest any large amounts of 'smoky gas' or particulates. The lack of contamination by ablation gases will be more comprehensively verified when the canister filter is disassembled and its contents studied.

Soil samples were also obtained and analyzed from the various SRC impact locations, as well as along the 'roll track'. Using LC-FD/TOF-MS, a suite of amino acids were detected in the soil samples including aspartic and glutamic acids, serine, glycine, β-alanine, alanine, γ-amino-*n*-butyric acid (GABA), ε-amino-*n*-caproic acid (EACA), and valine. Methylamine (MA) and ethylamine (EA) were not detected in the soil samples above the part per billion level. XANES analyses of the soil from the Stardust landing sight demonstrated that the soil contained carbonate, potassium, and unsaturated, aliphatic carbon molecules. Chloride (by IC) was very abundant, as expected, reaching 32 ppt. Sulfate (also by IC) was observed at approximately 3 ppm). The organic material was associated with the potassium containing particles all of which were less than one micron in size. Very little mud stuck to the SRC.

It does not appear that the Wild 2 samples suffered any contamination from soil or water at the recovery site and currently no indications exist that ablative gases from the heatshield were ingested into the sample canister.

However, the possibility remains that some of the returned cometary samples could have been contaminated by organics emplaced during manufacture, testing, launch, and cruise of the spacecraft, as well as during sample curation. Additional contaminants could also be present in the aerogel medium used to capture the cometary samples, although NMR measurements indicate the primary form of contaminant carbon in the aerogel is in the form of Si-CH_3 groups. These issues were investigated and assessed by exposing, collecting, and analyzing a series of 'witness' coupons during key phases of the mission, and by characterizing unflown portions of the aerogel batches located in the Stardust collection trays. Particularly important in this regard is the Flight Aerogel Witness Tile, a tile of aerogel that was mounted on the collector tray deployment arm. This aerogel was placed so that it was protected from impacts during the comet flyby by the spacecraft's dust shields. Thus, this tile witnessed all the same environments (terrestrial and space) as the cometary collector tiles, but did not see the comet. It therefore represents an ideal control sample for our organics investigations. Results from the examination of this tile are discussed in the individual technique sections.

Tests of the Alteration of Organics when Fired into Aerogel

Tests using standards fired into Stardust-like aerogels at velocities near 6 km/sec suggest that the degree of alteration of organic materials is very dependent on the nature of the organic material and the matrix material in which the organics are bound. L^2MS studies of test shots of pure PAHs, like pyrene, show the impact distributes material all along the track, and even a few track widths into the surrounding aerogel, but show little evidence of oxidation or other alteration of the original PAH. Thus, materials of this sort may be partially volatilized, but do not appear to be altered.

In comparison, L^2MS studies of shots of Allende meteorite (CV3) material showed very little of the organic matter was volatilized and deposited along the impact track. Analysis of multiple terminal particles in the tracks showed that, while the overall abundance of PAHs was reduced somewhat, the actually mass distribution was remarkably similar to that characteristic of unshot bulk Allende (CV3) *(S23)*. Again, it appears that aromatic materials are not greatly altered by impact into aerogel at these velocities, but that some material may be lost from the terminal particles.

In contrast, cocoa powder mixed with small soda-lime glass spheres and fired into aerogel shows a different behavior. In this case, essentially none of the original organics were found in association with the terminal soda-lime glass spheres; all the organic matter was found distributed along the bulb-shaped track and at least several track widths into the surrounding matrix (much like the shots of pure PAHs). However, in this case there was evidence of extensive alteration of some of the molecular components of the original cocoa powder, both in the form of bond-breaking and bond-creation. [NOTE: the segregation of organics and the glass in this case may explain why TEM analyses of removed grains show a relative dearth of organic materials adhering to mineral grains compared to what is seen for stratospheric IDPs].

Similar variations in the degree of alteration of organic materials fired into aerogels at these velocities are seen using other analytical techniques *(S24).*

Thus, one would anticipate that the organics in the collected cometary material could have undergone differing degrees of alteration ranging from little to no alteration all the way to extensive alteration, depending on the physical nature of the impacting particle and the chemical nature of the organics. Given the nature of many of the impacting particles (aggregates of smaller grains), it is possible that this entire range of degrees of alteration might be found in a single impact. In this respect, material in the tracks may share a characteristic of stratospheric IDPs, were individual particles can show evidence of severe heating and yet still retain some unmodified, less refractory materials. It should be noted, however, that the relatively heterogeneous and unequilibrated nature of many of the organics seen in the samples suggests that much of the material that has been examined has not been extensively altered by the collection process (see the main body of the paper).

Two-step laser desorption laser ionization mass spectrometry (L^2MS)

The L^2MS technique is ideally suited to the *in situ* detection of organic species that contain aromatic or π-conjugated systems *(S8)*. Such species, particularly in the form of the polycyclic aromatic hydrocarbons (PAHs), are believed to be ubiquitous in the interstellar and interplanetary environments *(S7,S15,S25)*. The L^2MS technique has been used to establish the presence of aromatic hydrocarbons in a wide variety of extraterrestrial materials including: meteoritic acid residues *(S26)*; carbonaceous and ordinary chondrites *(S27,S28)*; Martian meteorites *(S29)*; Antarctic micrometeorites *(S9)*; interplanetary dust particles *(S7)*; interstellar graphite grains *(S30)*; and interstellar ice analogs *(S31)*.

A detailed description of the μL^2MS technique has been presented in the literature *(S8,S26)* and is summarized here. Constituent neutral molecules of the sample are first desorbed with a pulsed infrared laser beam focused down to a spot, presently adjustable between 10 and 40 µm. Laser power density is maintained well below the plasma threshold to ensure desorption of neutral organic species with little or no fragmentation. A selected class of molecules in the desorbed plume is preferentially ionized by a single-frequency pulsed ultraviolet (UV) laser beam that passes through the plume. Resultant ions are then extracted and injected into a reflectron time-of-flight mass spectrometer and analyzed according to mass. A complete mass spectrum is obtained for each shot. The μL^2MS system at Stanford typically uses an ionization wavelength of 266 nm, which is strongly absorbed by the phenyl moiety and provides a selective ionization window for PAHs. The μL^2MS technique requires minimal sample processing and handling, and therefore allows analysis of samples with little possibility of contamination. Cometary impact tracks were exposed for μL^2MS surface analysis using the keystone extraction technique. All sample extractions were performed by Andrew Westphal, Christopher Snead, and Anna Butterworth in their UC-Berkeley Space Sciences Laboratory. In this technique, the track is dissected along its central axis *(S6)*. The resulting keystone was then mounted onto a brass sample platter using tape adhesive. Spatial analysis was performed using the Stanford University μL^2MS by rastering the laser desorption beam over the surface of the dissected track and using the NASA-JSC ultra-L^2MS to examine individual exposed particles. This results in complete mass spectra at each desorption spot (Fig S1 and S2).

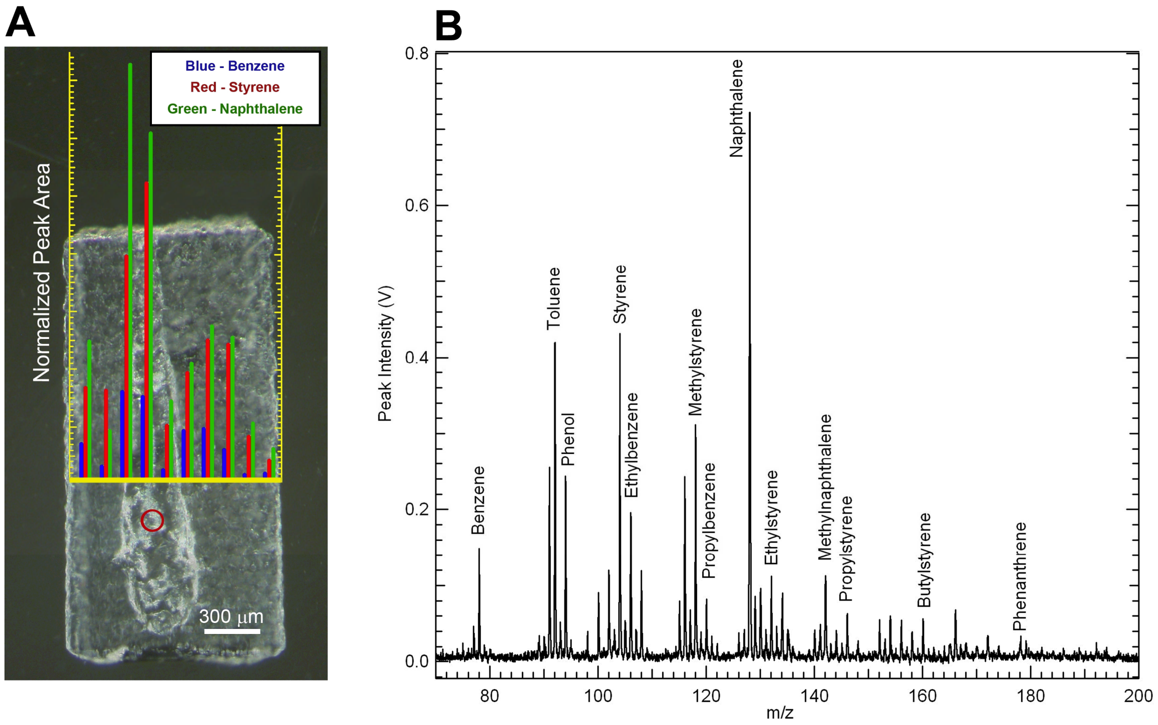

FIGURE S1 – μL^{2}MS of a cometary particle track in aerogel (Track 22): **(A)** the spatial distribution of three aromatic hydrocarbons whose intensities are plotted in a corss-section (in yellow) perpendicular to the cometary particle track. Aromatic molecules are found concentrated in the track, but also occur some distance on either side. **(B)** a mass spectrum taken within the cometary particle impact track at the location indicated by the red circle. Tentative peak identifications are listed mear major mass peaks. This low-mass distribution of aromatic compounds is typical of the entire track.

Low-mass PAH distributions are seen in flight aerogel not associated with impact tracks. The flight Aerogel Witness Coupon, an aerogel tile that was exposed to everything the rest of the tray was exposed to *except* the comet, showed even weaker PAH backgrounds. Both non-track cometary aerogel and the witness coupon aerogel show only a very weak indication of PAHs except at very high laser desorption powers. At high powers the μL^{2}MS CO_2 laser was observed to make a visible hole in aerogel samples and a stronger aromatic signature resulted. The presence of strong aromatic signals consistently correlated with the creation of a hole. No correlation between aromatic abundance and depth into the witness coupon was observed, indicating that the source of this material is distributed throughout the tile. At these higher powers both the cometary aerogels and the witness coupon produced identical aromatic signatures, indicating that this material is *neither cometary nor contamination introduced during space flight*. At these high powers, it is likely that the majority of the PAHs being seen in aerogel are due to pyrolysis of carbon in the original aerogel tiles. It is possible that these PAHs could also be created during the high energy impact of a small particle.

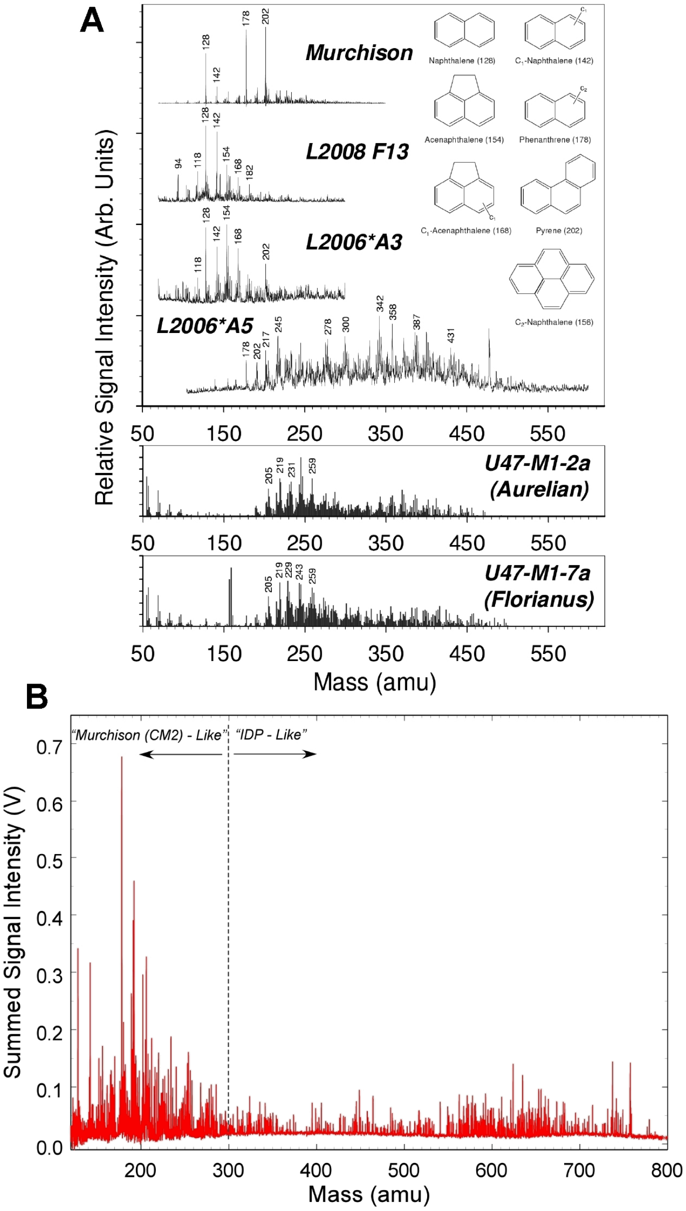

FIGURE S2 – (A) The L^{2}MS spectra of the carbonaceous chondrite Murchison and 5 stratospheric IDPs *(7)*. The meteorite and some IDPs show relatively simple populations dominated by small PAHs, but the spectra of some IDPs extend to higher masses, indicating a more complex distribution of PAHs. (B) The L^{2}MS spectrum of Stardust sample Track 16, is similar to the lower IDP spectra in 1A. The higher mass envelope of peaks above 300 amu for the Stardust sample probably reflects increased polymerization during impact with the aerogel compared to the more benign atmospheric deceleration experienced by most stratospheric IDPs.

Time-of-Flight Secondary Ion Mass Spectrometry (TOF-SIMS)

A TOF-SIMS IV instrument from ION-TOF was used in this study. The instrument is equipped with a pulsed gallium liquid metal ion source producing primary ions with 25 keV energy. Sample charging due to the primary ion beam is effectively compensated by bombardment with low-energy electrons between consecutive primary ion pulses. This allows all different types of Stardust samples to be studied without special sample preparation: crater residues on aluminum foil, dissected aerogel keystones displaying particle tracks, and extracted particles that were embedded in epoxy and sliced with a microtome. Since elements, isotopes, and organics as well as their lateral distribution were measured simultaneously in a single analysis, all measurements of Stardust samples were performed at high lateral (~0.2 µm) and high mass resolution ($m/\Delta m_{\mathrm{FWHM}} > 4000$ at mass 29 amu for rough surfaces like Al foil craters or aerogel tracks and ~5500 for flat surfaces like microtomed particles). Further details on TOF-SIMS technique are given in the literature *(S20)*.

TOF-SIMS detected PAHs that were clearly correlated to cometary material or impact feature as exemplified by a PAH secondary ion distribution image of a cometary impart crater found in aluminum foil sample C2009N (Fig S3b,c).

TOF-SIMS measurements of PAHs typically show fragmentation of PAHs. In most cases the $C_9H_7^+$ secondary ion has the highest abundances among all PAH ion peaks. The abundances of different sized PAHs relative to the abundance of $C_9H_7^+$ are similar for PAHs in tracks and terminal particles in aerogel, but show a flatter distribution in the residues found in craters in aluminum foil (Fig S3a). This may be a fractionation effect associated with a greater loss of small PAHs in the foil impacts.

PAHs from particles of the carbonaceous chondrite Allende shot into aerogel and analyzed in a dissected keystone *(S32)* show a size-abundance distribution of PAHs that is very similar to that seen in the cometary samples collected in aerogel. PAHs from the carbonaceous chondrites

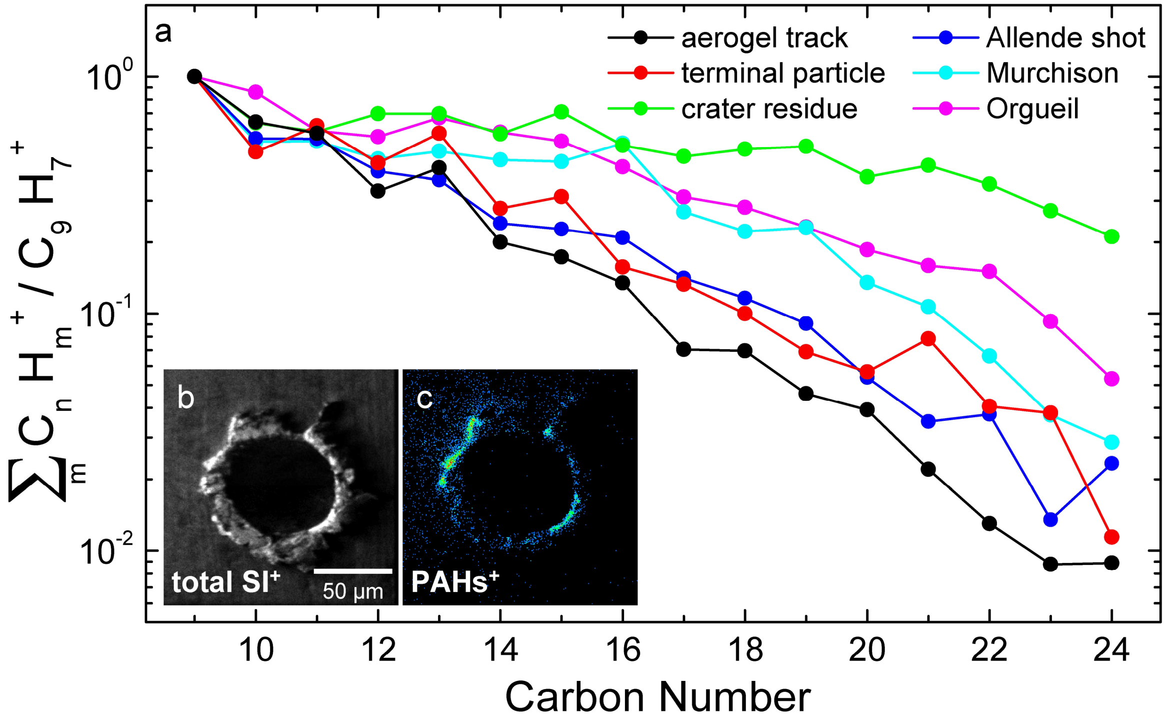

FIGURE S3 – (a) Abundances of PAHs in Stardust samples as a function of their number of carbon atoms relative to the abundance of $C_9H_7^+$, the PAH fragment that typically shows the highest intensity in TOF-SIMS analysis. Analyzed samples include one dissected aerogel keystone with a particle track (Track 21), one terminal particle extracted from aerogel (Track 44, Grain 4), and residue from the rim of a crater in aluminum foil (large crater from C2009N). For the latter, the corresponding PAH secondary ion distribution image (c) and a total secondary ion image (b) are shown. For comparison, data are also shown for Allende material shot into aerogel *(33)* and two carbonaceous meteorites, Murchison and Orgueil *(34)*.

Murchison and Orgueil meteorites show a somewhat higher relative abundance of heavier PAHs (see Fig S3a; *(S33)*).

Raman Spectroscopy

Raman spectra taken at the Osservatorio Astrofisico di Catania in Italy were taken from grains extracted from aerogel and deposited as bulk particles on KBr windows mounted in a special sample holders designed to allow combined micro-IR, micro Raman, FESEM, and EDS analyses without the need for sample manipulation in the laboratory *(S18)*. A Cu finder grid, with a central 300 μm hole was used to help localize the particle's location. A polycarbonate probe clip was placed over the Cu grid to serve as a clean shield to prevent spurious dust deposition and other contamination.

Raman spectra of 3 grains (Track 35, Grain 16; Track 35, Grain 18; and Track 35, Grain 20) were taken using a continuous multiline Ar ion laser beam at 514.5 nm wavelength. A confocal microscope (DILOR) focuses the laser beam onto the particle in a 1 μm diameter spot with a power mostly maintained at 0.03 mW and always lower then 0.1 mW. The Raman scattered light arising from the illuminated spot is collected by the same objective and is collimated into a parallel beam that is reflected back along the same path as the laser. The Raman scattered light is then focused on the entrance slit of the triplemate spectrometer (SPEX) equipped with a CCD detector. This confocal system makes it possible to perform measurements on samples with negligible performance losses.

Raman analyses at the Carnegie Institution of Washington were performed with a multi-function scanning probe microscope of the Geophysical Laboratory. The instrument, a WiTec (Germany) α-SNOM, includes near-field optical microscopy, atomic force microscopy and confocal Raman microscopy (532 nm frequency-doubled Nd:Yag laser). The instrument allows non-destructive Raman characterization of samples at sub-μm spatial resolution (typically ~400 nm with 100x short working distance optical microscope). Spectral images were acquired, where each pixel contains a full Raman spectrum (1024 channels, 600 gratings/mm, ~4 cm^{-1} spectral resolution). The Raman data cube was reduced using custom software. Tests have shown that meteoritic insoluble organic matter has not been significantly altered during the analyses, due to the laser-induced heating at low power (55 μW) and the fast measurements (typically 4 sec/pixel). Excessive fluorescence overwhelming Raman spectral features has been overcome with the use of confocal optics. All samples (Track 13, Grain 1; Track 35, Grain 25; Track 35, Grain 27; Track 17, Grain 1) were pressed into gold and most particles were subsequently analyzed with SIMS (Track 17, Grain 1 was analyzed after the SIMS measurements).

Laser Raman analyses were conducted at PSSRI, Open University, on Samples Track 35, Grain 1, and Track 35, Grain 28. These samples were particles (aerogel with some cometary material) extracted and pressed into gold foil at NASA-JSC. Laser Raman data were taken with a fully confocal Horiba Jobin Yvon Labram HR Raman system. The laser, a 514 nm argon ion laser, delivered a power at the sample surface of 180 μW (Track 35, Grain 28) and 60 μW (Track 35, Grain 1). The beam was focused with a x100 long working distance objective giving a spatial resolution of approx 1.2 μm. Spectra were recorded across the whole of each particle with a 1.5 μm step in both x and y. Spectra were accumulated as 5 sets of 30-second integrations. The 800 mm spectrometer coupled with a low resolution grating gives a dispersion of 2 cm^{-1} per pixel on the CCD detector at 514 nm. The instrument was calibrated for absolute laser wavenumber and Raman shifts before analyses. The steep sloping fluorescence baseline was subtracted and the D and G features fitted with a Gaussian-Lorentzian model.

Raman spectra obtained by the Orsay–IAS group were taken from grains extracted from aerogel and pressed as bulk particles on gold windows, allowing, without the need for sample manipulation, combined micro-IR, micro Raman, FESEM, and EDS non destructive analyses and followed by a NanoSIMS investigation of the same grains. The Raman instrument is a Labram HR800 Horiba Jobin-Yvon (national facility equipment at ENS Lyon). Excitation is delivered by an argon ion laser (514.5 nm) and the spectral resolution is of 1 cm^{-1} when using a 1800 gr/mm grating. The laser power at the sample surface did not exceed 0.1 mW. The spatial resolution is 1 μm when using a x100 Olympus objective. The analytical procedure consists in fitting the D and G bands with two Lorentzian bands and a linear baseline.

Raman measurements at Washington University in St. Louis were performed on sample Track 35, Grain 30 that was pressed into Au at NASA-JSC (Fig S4). The instrument used is an integrated, fiber-optically coupled microscope-spectrometer-detector system (HoloLab Series 5000 Raman Microscope from Kaiser Optical Systems, Inc). This instrument has no moving parts and is based on an axial spectrometer with holographic gratings that allows for very good photon efficiency and wavelength accuracy. Raman excitation light of 532 nm is delivered by a frequency-doubled Nd-YAG laser that was coupled into a Leica microscope via a 8 μm single mode optical fiber. A 80x ULWD objective with NA of 0.75 and a working distance of 8 mm was used for focusing the light onto the sample, which resulted in a spatial resolution of ~1 μm. The laser power at the surface of the sample was less than 500 μW. The spectral range of 100-4000 Δcm^{-1} was simultaneously detected with a thermoelectrically-cooled CCD array detector with 2048 channels and a spectral resolution of 2.5 cm^{-1}. Spectral acquisition time was 64 x 4 seconds per spectrum. Data acquisition, intensity and wavelength calibration, as well as filtering were controlled by the HoloGrams software. Peaks were deconvolved with a mixed Gaussian-Lorentzian algorithm without any baseline correction.

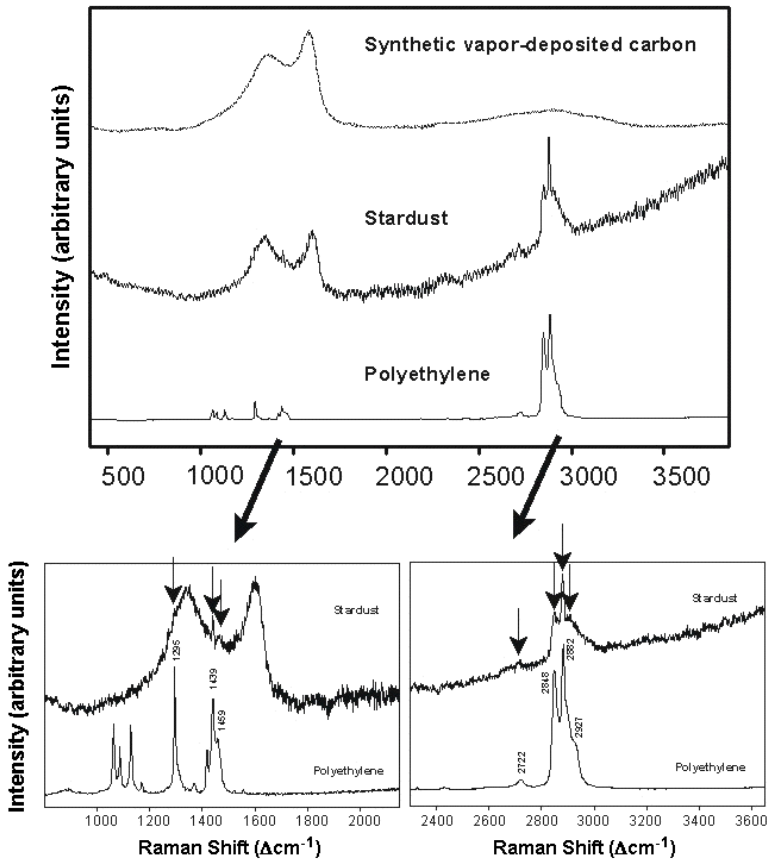

FIGURE S4 – The background corrected spectrum of the Stardust particle (Track 35, Grain 30) shows bands for both aromatic and aliphatic carbonaceous materials. The two very broad bands centered at ~1360 Δcm^{-1} (D band) and ~1590 Δcm^{-1} (G band) are caused by aromatic C-C vibrations characteristic of large PAHs or in kerogen-like materials. While the Raman data of Stardust samples are uniformly dominated by the aromatic G and D bands, this particle was seen to also produce strong C-H stretching vibration peaks at 2848 and 2882 Δcm^{-1}, and a weak band at 1439 Δcm^{-1}. These features are consistent with the presence of alkane-type saturated hydrocarbons, as exemplified by comparison with the spectrum of polyethylene. Similar aliphatic features were also seen in Raman spectra of two additional Stardust samples (Track 35, Grain 32 and Track 41, Grain 11 generally seen in Raman spectra of Stardust samples.

Infrared Spectroscopy

Infrared spectra were obtained from the infrared microspectroscopy beamline 1.4.3 at the Advanced Light Source, Lawrence Berkeley National Laboratory. This beamline was used to map distribution of organics in and around particle tracks within aerogel keystones. The beamline is equipped with a ThermoNicolet Magna 760 FTIR bench and a SpectraTech Nic-Plan IR microscope. The synchrotron source was focused to a diffraction-limited spot and aligned with the optical beam path. For the measurement of the $-CH_2-$ and $–CH_3$ peaks this corresponds to a spot size of ~3 µm. A KBr beamsplitter was placed in the beam path and the transmitted light was collected with an MCT-A detector between 650 and 4000 cm^{-1} with 4 cm^{-1} spectral resolution. Spectra were normalized to the air spectrum and typically collected between 6-60 sec/point. Aerogel keystones (100-200 µm thick) were held with microtweezers and placed directly under the microscope. The sample, mounted on a special sample holder, was moved on a microscope stage with sub-micrometer precision while the beam remained fixed during data collection of the maps.

Infrared spectra were also acquired at the Osservatorio Astronomico di Capodimonte in Italy with a microscope attached to a FTIR interferometer (Mod. Bruker Equinox-55) in the range 7000-600 cm^{-1} with a spectral resolution of 4 cm^{-1}. Comet Wild 2 particles (Track 35, Grain 16; Track 35, Grain 18; Track 41, Grain 7, and Track 41, Grain 10) were placed on a special sample holder *(S18)* and spectra acquired in transmission. Due to diffraction limits, the smallest infrared beam focused on the samples was 20 µm spot. This was larger then the average size (about 10 µm) of the analyzed particles. Thus, spectra of overall bulk particles were obtained.

FTIR spectra obtained by the Orsay–IAS group were taken from the same grains from which Raman spectra were acquired. The instrument is a NicPlan microscope associated with the Magma 860 FT-IR spectrometer equipped with MCT detectors and used in the reflection mode. The IR source is an internal globar type source; KBr beamsplitters are available in the 5000–500 cm^{-1} range. The wavelength/wavenumber coverage is 2.5–15.4 µm (4000–650 cm^{-1}) with a spectral resolution of 4 cm^{-1}. The smallest IR beam focused on the samples was around 15 µm, the approximate size of the samples.

Fig S5 shows the 4000-1500 cm^{-1} infrared spectrum of sample Track 59. This spectrum contains features due to both sample material and aerogel. Calculating the relative abundance of functional groups detected in the IR spectra, particularly the $-CH_2-$ and $-CH_3$ groups, requires that absorption contributions from the aerogel be removed. This can be done by subtracting the spectrum of aerogel far from a track to the sample spectra. Fig S6 shows an example where this has been done in the OH and CH stretching region. The corrected spectrum shows an aliphatic CH stretching feature centered near 2900 cm^{-1} that is clearly dominated by $-CH_2-$ groups. A weak aromatic CH stretching band is also seen near 3055 cm^{-1}. Since aromatic structures can have relatively low H coverage (particularly compared to aliphatic materials), the relative weakness of this feature does not necessarily imply low abundances of this material.

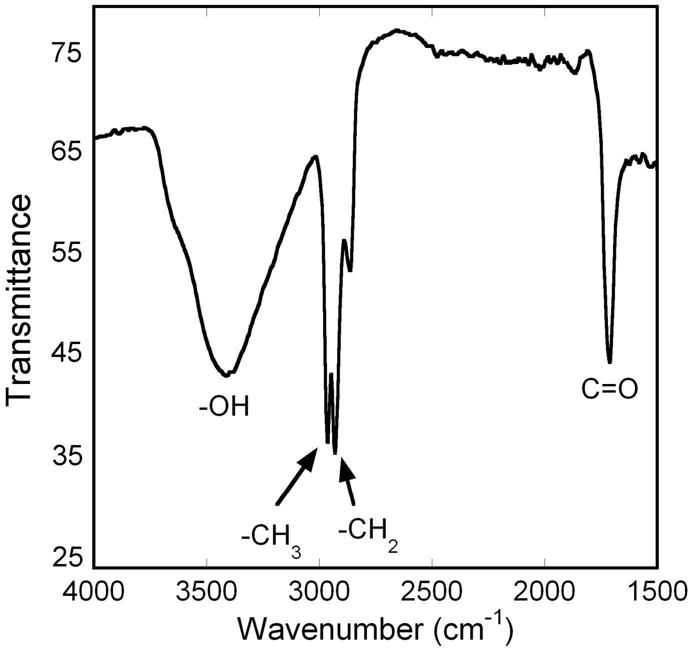

FIGURE S5 – The 4000-1500 cm^{-1} infrared spectrum of a section of Track 59. Absorption features can be seen near 3322 cm^{-1} (–OH), 2968 cm^{-1} ($-CH_3$), 2923 cm^{-1} ($-CH_2-$), 2855 cm^{-1} ($-CH_3$ and $-CH_2-$), and 1706 cm^{-1} (C=O). All these features except the 1706 cm^{-1} C=O band contain some contributions from aerogel.

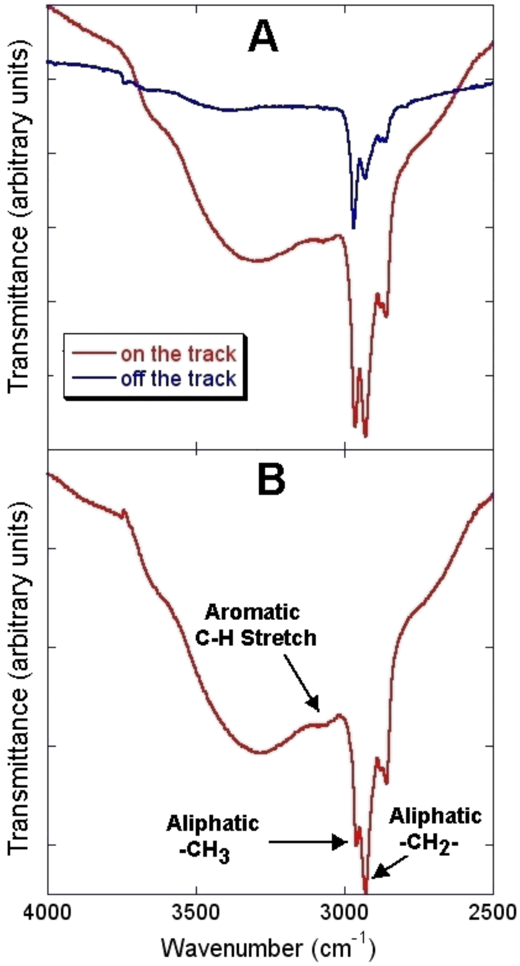

FIGURE S5 – (A) The 4000-2500 cm^{-1} spectrum from an aerogel keystone (Track 58) on a track (red line) and far from the track (blue line). The aerogel spectrum can be scaled using an absorption feature due solely to aerogel and subtracted from the track spectrum. The residual absorption (B) is then dominated by new, non-aerogel material associated with the track dominated by a broad feature near 3300 cm^{-1} (-OH) and narrower features near 3065 cm^{-1} (aromatic CH stretch, weak), 2968 cm^{-1} (-CH_3 asymmetric stretch), 2923 cm^{-1} (-CH_2- asymmetric stretch), and 2855 cm^{-1} (symmetric -CH_3 and -CH_2- stretches).

Scanning Transmission X-ray Microscopy and X-ray Absorption Near Edge Structure (STXM/XANES)

XANES of ultramicrotomed sections of particles extracted from aerogel were performed on three different STXMs located at beam lines 5.3.2 and 11 at the Advanced Light Source, Lawrence Berkeley Laboratory, and beam line X1A at the National Synchrotron Light Source, Brook Haven National Laboratory. XANES analyses can provide information regarding the oxidation state and bonding environments of low Z elements (C, N, and O). When combined with STXM, micro-XANES may be acquired at spatial resolutions down to 100's of nanometers *(S12)*, thus affording a unique opportunity to explore organic chemical variation in retrieved aerogel particles. Also, by using a method where a series of x-ray images taken at incremental differences in the photon energy are collected and spatially aligned, one can obtain spectra from regions as small as the spatial resolution of the microscope (30 nm) *(S34)*.

The Scanning transmission x-ray microscopes used in this study use coherent radiation from a synchrotron light source, ranging in energy from 100-1500 eV. This light is monochromatized and focused to a spot using a Fresnel zone plate. The typical focus spot for this work was 30 nm. The sample is scanned through the focus and the transmitted intensity is recorded by a large area detector, resulting in an absorption contrast image of the sample. The energy of the microscopes are well matched to the inner-shell electron binding energy of low Z elements, resulting in high absorption coefficients and high quality contrast images. Using spectromicroscopy, one can obtain a series of images of the same field taken at different energies around an element's absorption edge. From these energies at and away from an element's x-ray absorption near edge structure (XANES) resonances, different bonding states of that element can be identified. XANES spectroscopy corresponds to the transition of an electron from a core-level to an unoccupied virtual orbital or continuum and reflects the electronic state of the atom. Its capabilities are: 1. the detection of bonds (C-C, C=C, C=O, and C-H, to name a few); 2. the determination of bond lengths; and 3. crystal orientation *(S35)*.

The relative C, N, and O abundance of the XANES samples can be determined by measuring the X-ray absorption intensity above the respective C-, N-, and O- 1s ionization edges, which correlates with the atomic density of each element in the sample. This works well if there is no significant contributions in the absorption spectra from other elements having binding energies from other electron shells besides the K shell. Fig S7 shows C-, N-, and O- 1s ionization edge spectra of a Stardust sample.

Materials with the high O/C and N/C ratios typical of the organic materials examined by XANES are likely to be relatively labile, and there is ample evidence seen for this. First, of course, is the observation from infrared spectroscopy that organics have been injected into the aerogel surrounding many of the impact tracks. In addition, in the case of XANES measurements, a number of instances were observed in which the organic material, or a portion of it, disappeared as it was measured in the X-ray beam. This was observed during measurements with higher X-ray fluences. Similar behaviors were also seen in other beam instruments (for example, Nano-SIMS). Also, in one case (a thin section from Track 35, Grain 16, Mount 4), evidence is found for organic matter that diffused out of the original particle and into the surrounding epoxy in which the particle was embedded for microtoming, suggesting that a portion of the organics are soluble in epoxy.

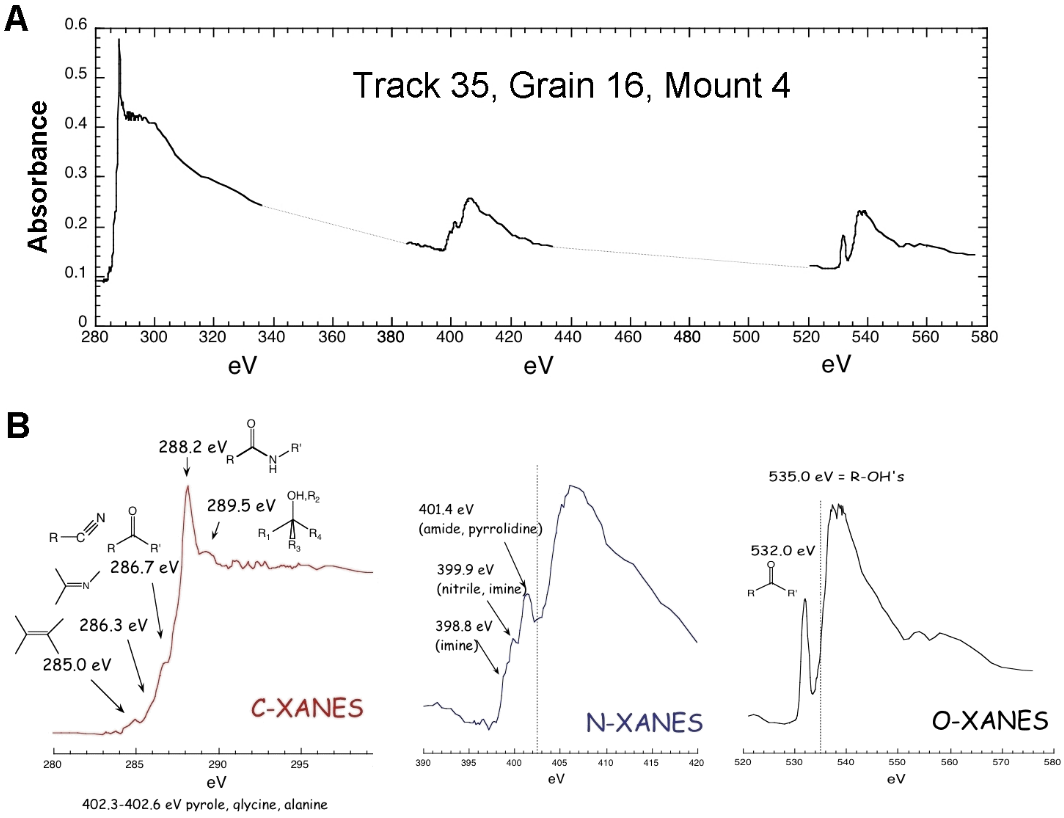

FIGURE S7 – (A) A XANES spectrum showing the C-, N-, and O- 1s ionization edges of Track 35, Grain 16, Mount 4 to scale. The relative intensity of each edge at energies beyond each near edge region is directly related to the relative atomic abundance of each element. (B) Expanded spectra of the individual C, N, and O edges revealing the near edge spectral features associated with different organic functional groups..

Liquid Chromatography with UV Fluorescence Detection and Time of Flight Mass Spectrometry (LC-FD/TOF-MS)

We investigated the abundances of amino acids and amines, as well as their enantiomeric composition, in Stardust flight aerogels (Cell 2054, Aerogel Fragment 4, hereafter C2054,4, and Cell 2086, Aerogel Fragment 1, hereafter C2086,1) using high performance liquid chromatography with simultaneous UV fluorescence and time of flight-mass spectrometry detection (LC-FD/TOF-MS). The LC-FD/TOF-MS were identical to those described in *(S10)*. Three pieces (1-3) of the C2054,4 were cut from the original slab (Fig S8) and weighed separately with masses of 5.2 mg, 7.6 mg, and 8.7 mg, respectively. Piece 3 was located directly under and adjacent to Piece 5, which contained Track 25 (Fig S8). C2086,1 weighed 3.2 mg and was taken from Tile C2086 from a location that was not adjacent to any visible impact tracks. As controls, procedural blanks and several Stardust aerogel samples, including a 14 mg piece of preflight aerogel (Flight Spare Aerogel Cell E243-13C, unflown) that had been kept sealed under vacuum since original bakeout in 1998 and a 0.2 mg sample of the aerogel witness coupon (WCARMI1CPN,9), were carried through the same extraction protocol. The aerogel samples were heated inside a sealed glass ampoule containing 1 mL Millipore water (18 MΩ) at 100ºC for 24 h. The water extracts were dried under vacuum and half of each extract was then hydrolyzed under 6M HCl vapor at 150ºC for 3 h. Both acid hydrolyzed and non-hydrolyzed aerogel water extracts were derivatized with *o*-phthaldialdehyde/*N*-acetyl-L-cysteine (OPA/NAC) and analyzed for primary amines using LC-FD/TOF-MS.

The most abundant primary amine compound detected in the Stardust flight aerogels is ε-amino-*n*-caproic acid (EACA); its most likely origin is exposure to Nylon-6 *(S10)*. Several other amines including glycine, β-alanine (BALA), γ-amino-*n*-butyric acid (GABA), L-alanine, ethanolamine (MEA), methylamine (MA), and ethylamine (EA) were also identified in the aerogels (Fig S8). The absence of D-amino acids and the similarity in amine distribution between the comet exposed C2054,4 sample and the witness coupon indicates that most of the amines are terrestrial in origin (Fig S8). The enhanced relative abundances of MA, EA, and possibly glycine in both comet-exposed aerogel samples compared to the preflight and witness

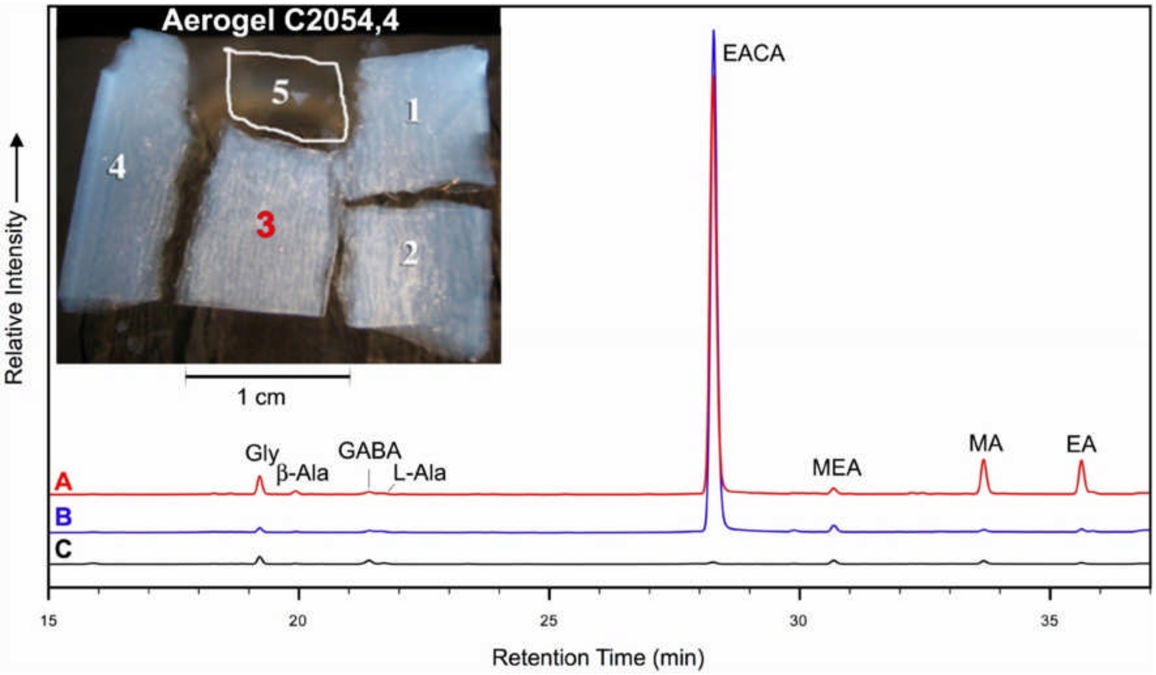

FIGURE S8 - The fluorescence chromatograms from LC-FD/TOF-MS analyses showing the amines detected in: (A) Stardust comet exposed aerogel C2054,4-Piece 3; (B) Stardust aerogel witness coupon WCARMI1CPN,9; and (C) preflight aerogel (Flight Spare Aerogel Cell E243-13C, unflown). Peak identities were established by comparing retention time with authentic standards and measuring the positive electrospray exact mass of each identified peak. The inset shows the C2054,4 cutting diagram oriented with the comet-exposed surface at the top. MA and EA were detected in aerogel Pieces 1-3 at levels that exceeded those found in the aerogel witness coupon and preflight aerogel. There was no significant difference in MA and EA abundances between Pieces 1 and 2 to suggest a concentration gradient with depth. Pieces 4 and 5 (which contained Track 25) were not analyzed by this technique.

coupon aerogels suggest a cometary origin for these compounds (Fig S9). Compound specific isotopic analyses of these amines will be necessary to constrain their origin.

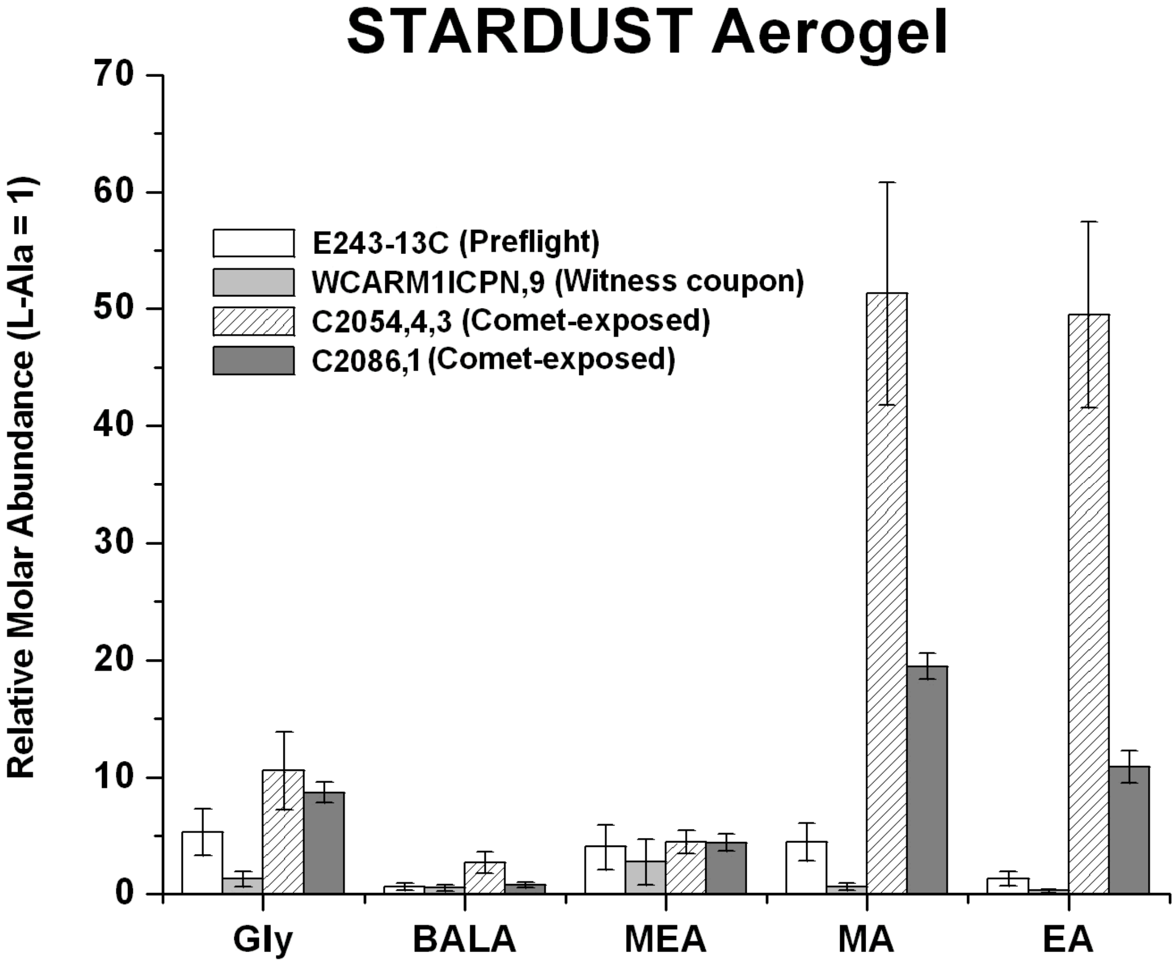

FIGURE S9 - A comparison of the relative molar abundances (L-Ala = 1) of glycine (Gly), β-alanine (BALA), ethanolamine (MEA), methylamine (MA), and ethylamine (EA) in the acid-hydrolyzed hot-water extracts of Stardust aerogel. The high relative abundances of MA, EA, and glycine in comet-exposed aerogel samples C2054,4 (Piece 3) and C2086,1 compared to the preflight (E243-13C) and witness coupon (WCARM1ICPN,9) aerogel samples suggest a cometary origin for these amines.

Secondary Ion Mass Spectrometry (SIMS)

Hydrogen isotopes were measured along with C using a Cameca ims-6f ion microprobe, in scanning imaging mode. A focused <10pA Cs^+ ion beam was rastered across samples with synchronized collection of secondary ions. Techniques were identical to those described in *(S36)*. All but one analyzed sample were extracted from the aerogel collectors and pressed into Au foils. A 500 nm thick slice of sample Track 13, Grain 1, prepared by ultramicrotome, was placed directly on a Au foil. Data were quantified using custom image processing software and terrestrial standards.

Chemical maps of Stardust samples were produced with the Cameca NanoSIMS 50 of the Muséum National d'Histoire Naturelle in Paris. Samples were placed on a gold foil. Using a focused primary beam of Cs^+, secondary ions of $^{12}C^-$, $^{12}C^{14}N^-$ and $^{32}S^-$ were sputtered from the sample surface and detected simultaneously (multicollection-mode) in electron-multipliers at a mass-resolving power of ~4500 ($M/\Delta M$). At this mass-resolving power, the measured secondary ions are resolved from potential interference. Because nitrogen is detected as CN^-, it can only be detected in the presence of carbon. Images were obtained from pre-sputtered surfaces by stepping the primary beam across the sample surface. The primary beam was focused to a spot-size of ~50-100 nm and the step-size was adjusted so that it was comparable to, but slightly smaller than the size of the primary beam. An electron gun supplied electrons to the sputtered surface during analysis in order to compensate positive charge deposition from the primary beam and minimize charging effects.

Calibrated N/C atomic ratios were obtained from the measured $^{12}C^{14}N^-$ and $^{12}C^-$ ratios by normalization to a kerogen standard from the Eocene Green River Shale. The kerogen was extracted by standard HF-HCl techniques and comprised $\geq$94% of the insoluble acid residue; it has an atomic N/C ratio of 0.025 (measured by standard chemical techniques), which was calibrated to the $^{12}C^{14}N^-/^{12}C^-$ ratios measured under NanoSIMS conditions identical to those used for analyzing the Stardust samples.

The Presence of Labile Organics

Several experimental groups observed the loss of organics in their samples over time when exposed to higher X-ray, laser, or ion beam fluences, providing further evidence of a relatively labile component of the organics. It is interesting to note that this may be one reason why organic grains appear to have low abundance in TEM sections *(S37)*.

References and Notes

S1. J. Kissel, F. R. Krueger, Nature 326, 755 (1987).

S2. M. J. Mumma, in Astronomical and Biochemical Origins and the Search for Life in the Universe, C. B. Cosmovici, S. Bowyer, D. Wertheimer, Eds. (Editrice Compositori, Milan, 1997), pp. 121-143.

S3. J. Oró, Nature 190, 389 (1961).

S4. E. Anders, Nature 342, 255 (1989).

S5. A. H. Delsemme, Advances in Space Research 12, 5 (1992).

S6. A. J. Westphal et al., Meteoritics Planetary Science 39, 1375 (2004).

S7. S. Clemett, C. Maechling, R. Zare, P. Swan, R. Walker, Science 262, 721 (1993).

S8. S. J. Clemett, R. N. Zare, in Proceedings of the IAU Symposium 178: Molecules in Astrophysics: Probes & Processes, E. F. Van Dishoeck, Ed. (Kluwer, Dordrecht, 1997), pp. 305-320.

S9. S. Clemett et al., Origins of Life and Evolution of the Biosphere 28, 425 (1998).

S10. D. P. Glavin et al., Meteoritics Planetary Science 41, 889 (2006).

S11. J. Kirz et al., Review of Scientific Instruments 63, 557 (1992).

S12. A. L. D. Kilcoyne et al., J. Synchrotron Radiation 10, 125 (2003)

S13. M. Lerotic et al., Journal of Electron Spectroscopy and Related Phenomena 144-147C, 1137 (2005).

S14. S. A. Sandford, R. M. Walker, R. M., Astrophys. J. 291, 838 (1985).

S15. L. J. Allamandola, S. A. Sandford, B. Wopenka, Science 237, 56 (1987).

S16. G. J. Flynn, L. P. Keller, M. Feser, S. Wirick, C. Jacobsen, Geochim. Cosmochim. Acta. 67, 4791 (2003).

S17. G. Matrajt et al., Astron. & Astroph. 433, 979 (2005).

S18. A. Rotundi et al., Workshop on Dust in Planetary Systems, in press.

S19. G. W. Cooper M. H. Thiemens, T. Jackson, S. Chang, Science 277, 1072 (1997).

S20. T. Stephan, Planet. Space Sci. 49, 859 (2001).

S21. K. D. McKeegan, R. M. Walker, E. Zinner, Geochimica et Cosmochimica Acta 49, 1971 (1985).

S22. P. Hoppe et al., Meteoritics Planetary Science 41, 197 (2006).

S23. M. Spencer, R. N. Zare, LPSC XXXVIII, 1432 (2006).

S24. M. J. Burchell, J. A. Creighton, A. T. Kearsley, Journal of Raman Spectroscopy 35, 249 (2004).

S25. J. Elsila, et al., Geochimica et Cosmochimica Acta 69(5), 1349 (2005).

S26. L. J. Kovalenko et al., Anal. Chem. 64, 682 (1992).

S27. J. H. Hahn, R. Zenobi, J. L. Bada, R. N. Zare, Science 239, 1523 (1988).

S28. R. Zenobi et al., Geochim. Cosmochim. Acta 56, 2899 (1992).

S29. D. S. McKay et al., Science 273, 924 (1996).

S30. S. Messenger et al., Astrophys. J. 502, 284 (1998).

S31. M. P. Bernstein et al., Science 283, 1135 (1999).

S32. T. Stephan, A. L. Butterworth, F. Hörz, C. J. Snead, A. J. Westphal, Meteoritics Planetary Science 41, 211 (2006).

S33. T. Stephan, E. K. Jessberger, C. H. Heis, D. Rost, Meteoritics Planetary Science 38, 109 (2003).

S34. J. Jacobsen, G. J. Flynn, S. Wirick, C. Zimba, Journal of Microscopy 197, 173 (2000).

S35. J. Stohr, NEXAFS Spectroscopy, (Springer Series in Surface Sciences, E. Gomer, Ed., New York, 1992).

S36. H. Busemann et al., Science 312, 727 (2006).

S37. M. E. Zolensky et al, this issue.

38. Acknowledgements –

The Organics PET is grateful for support and samples provided by the NASA Stardust Discovery Mission and the NASA Stardust Participating Scientist Program, and the wonderful support of the Stardust curatorial staff at Johnson Space Center, especially Keiko Nakamura-Messenger, Ron Bastien, Jack Warren, and Tom See.

Gas Chromatography/Mass Spectrometry work on the collected gas samples was done in the Toxicology Laboratory, Habitability and Environmental Factors Division, NASA-Johnson Space Center. The authors are particularly grateful for the efforts of M. Martin (Catholic University of America), V. de Vera (WYLE Laboratories), J. Boyd (WYLE Laboratories), T. Limero (WYLE Laboratories), and J. James (NASA-JSC).

Part of this work was performed under the auspices of the US Department of Energy by the Lawrence Livermore National Laboratory under Contract No. W-7405-ENG-48 and the Advanced Light Source, which is supported by the Director, Office of Science, Office of Basic Energy Sciences, Materials Sciences Division, of the U.S. Department of Energy under Contract No. DE-AC03-76F00098 at Lawrence Berkeley National Laboratory. We would like to thank Michael C. Martin and Z. Hao (LBNL) for their support at the beamline.

The Italian LANDS is grateful for support provided by the Università degli Studi di Napolit "Parthenope" and the Instituto Nazionale di Astrofisica.